Program FINAL REPORT

Project Title: Fissile and Non-Fissile Material Detection Using Nuclear Acoustic Resonance Signatures

Covering Period: May 17, 2004 – July 31, 2008

Date of Report: November 2008

Recipient: The Pennsylvania State University
212 Earth-Engineering Sciences
University Park, PA 16802

Award Number: DE-FG07-04ID14556

Awardee Name: Pennsylvania State University

Contact(s): Bernhard R. Tittmann and P. M. Lenahan (Co-P.I.s) The Pennsylvania State University
Department of Engineering Science and Mechanics
University Park, PA 16802

Project Team: David Spears, Rhys Williams

Project Objective:

The objective of this project is to develop a novel technique for remote, non-destructive, non-radiation-based detection of materials of interest to Nonproliferation Programs, i.e., ^{235}U and ^{239}Pu. We propose the development of a detection system based on magnetic resonance principles (NAR), which would work where radiation detection is not possible. The approach would be non-intrusive, penetrating, applicable to many materials of interest for Nonproliferation, and be able to identify the nuclear samples under investigation. Nuclear Acoustic Resonance (NAR) is similar to Nuclear Magnetic Resonance (NMR) in that it induces transitions at resonances between energy levels that are defined by the interactions of electric and magnetic properties of nuclei with internal and external magnetic fields, electric quadrupole moments, and electric field gradients. Unlike NMR, which utilizes RF radiation, NAR uses acoustic radiation to induce transitions between energy levels. The acoustic modulation of internal interactions involving the magnetic and electric multipole moments of the nucleus is potentially observable by nuclear or electron spin transitions. The feasibility of this approach is first being determined at The Pennsylvania State University (PSU) with low Z, but high spin materials, including aluminum, lithium in oil, cesium, and indium. An initial estimate of the advantage and limitations of this approach for materials of interest containing the presence of ^{235}U and ^{239}Pu will occur with collaboration between the PSU and Lawrence Livermore National Laboratory (LLNL). If successful, the project will be transferred to LLNL, where NAR techniques will be performed on special materials of interest. *The development of this system could have enormous potential as a complementary means for detecting and identifying concealed fissile materials, useful in circumstances where*

radiation detection is impractical.

Background:

We are developing a novel technique, Nuclear Acoustic Resonance (NAR), for remote, non-destructive, non-radiation-based detection of materials of interest to Nonproliferation Programs, including ^{235}U and ^{239}Pu. This new technique uses the unique NAR signatures generated by acoustic excitation of phonon modes via ultrasound. The acoustic modulation of internal interactions involving the magnetic and electric multi-pole moments of the nucleus is potentially observable by nuclear or electron spin transitions. If successful, the project will be transferred to LLNL, where NAR techniques will be performed on actual samples of special nuclear materials. Since this technique does not rely on nuclear radiation detection, the eventual device objective would be to detect and identify fissile materials even if steps had been taken by smugglers to shield the materials as a radiation source. A successful device could have potential for the detection and identification of concealed fissile materials, a key and still unresolved issue facing nonproliferation and counterterrorism.

Status of Magnetic Resonance Studies

Although the first papers on NAR were published as far back as 1956 [1], the theory of NAR is still relatively new and has never been tried at the earth's magnetic field and at room temperature. NAR was developed at the same time as Nuclear Magnetic Resonance (NMR). However, NMR had the potential to obtain information about semiconductors and insulators, including biological systems, while NAR was more effectively used for probing conductors, where NMR is ineffective [2-10]. As NAR tools have increased in their ability to penetrate into conductors (i.e., acoustic transducers) and detectors have become more sensitive to electric and nuclear changes (i.e., Overhauser and potassium magnetometers and Superconducting Quantum Interference Device (SQUID) detectors), NAR might have the potential to be effective at room temperature and at the earth's magnetic field, making an NAR detector for ^{235}U and ^{239}Pu possible.

(1) Technical Approach

Our initial experiments will involve surrogate systems. In the simplest of cases, the Overhauser enhancement will occur for a nuclear species at a unique ratio of electron and nuclear resonance frequencies. $W_e=g_e ß_e H$ and $w_n=\gamma_n H$. In this, simplest of cases, the ratio of the two frequencies is essentially independent of the field of the sample when we study $w_n/w_e=\gamma_n/g_e ß_e$. Unfortunately, this will not be the case for ^{235}U, as the uranium nuclei possess quadrupole moments and the uranium crystal symmetry generates static electric field gradients.

(2) Results

From relatively simple calculations, discussed elsewhere we have shown that it is, at least in principle, possible to detect nuclear materials including ^{235}U with quite small applied field (i.e., Earth's Field) at room temperature. We are in the process of performing more extensive calculations to determine the theoretical limits of NAR for detecting ^{235}U, where the acoustics are in the non-contact mode.

In our first attempt to determine the sensitivity of a detector, we purchased an Overhauser magnetometer. We were able to observe periodic signals at sensitivities on the order of 10^{-11} Tesla per root Hertz, without signal averaging or a lock in amplifier. However, in order to observe NAR at room temperature in the earth's magnetic field, we need to achieve at the very least an order of magnitude increase in sensitivity. It will be very difficult to achieve the maximum sensitivity and also difficult to accurately

estimate how close we may be to such sensitivity. We purchased a customized potassium magnetometer, which utilizes phase sensitive detection, from GEM Systems, Inc. This system will eventually provide more than two orders of magnitude more sensitivity than the Overhauser magnetometer currently in use. We are in the process of testing this detector out. In order to further test out sensitivity, we have also purchased a SQUID detector to determine the ultimate sensitivity that we can obtain.

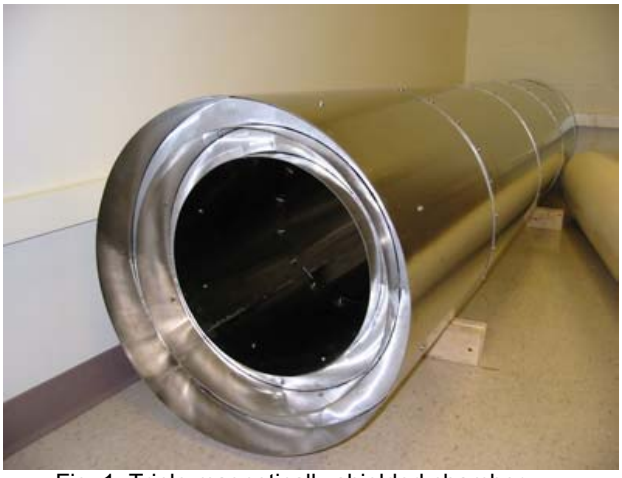
Fig. 1: Triple magnetically shielded chamber

In addition to increasing the sensitivity of the detector, we have also determined that both the Overhauser and potassium magnetometer require a very stable and homogeneous field in order to minimize the background noise. We have researched magnetically shielded chambers and carried out fairly extensive calculations on the (very highly uniform) magnetic fields which can be generated within a long cylindrical high permeability chamber with a solenoid. With the help of Ammuneal Corp., we have developed and obtained a three-walled magnetically shielded chamber, which is shown in Fig. 1. Students at PSU have designed and constructed simple, relatively inexpensive temperature compensated Hall Effect probes to monitor the small ambient AC and DC magnetic fields outside the magnetically shielded chamber. Students are also working on a magnetic field controller for the shielded chamber/solenoid/magnetometer system. These students have also built a large solenoid, which is shown in Fig. 2, to produce an extremely uniform static magnetic field with a magnetic field of up to 0.5×10^{-4} Tesla. Along with this large solenoid, these students have designed and built a circuit to provide a steady current supply for the uniform magnetic field.

Significant effort has also been made to minimize the amount of magnetic noise generated by the acoustics equipment since the Overhauser magnetometer requires a very stable and homogenous field to operate properly. Some of the main modifications include custom built transducers made with no casings, design and construction of a wooden sample holder (no nails), In order to determine the absorption and desorption produced by ultrasonic sound waves at both electronic and magnetic frequencies of metals, one needs to measure the change of ultrasonic attenuation and the change of ultrasonic velocity that is induced by ultrasonic sound waves in the metal. We have begun to measure these values with a Laser Doppler Vibrometer and begun to calculate the absorption and dispersion of ultrasonic sound wave in metals, including aluminum. We have started with samples of single crystal and polycrystalline aluminum, in order to test out our equipment. In order to maximize the amount of ultrasonic energy needed to induce changes in the metal to observe a NAR signal at the earth's magnetic


Fig. 2: The solenoid shielded chamber can provide extremely uniform static magnetic field with a magnetic field of up to1.8 Gauss

field, we have currently begun to develop computer simulation. We wish to observe the wave propagation in the metal and calculate strain/ displacement for a variety of frequencies, amplitudes, and samples. We are using these measurements to maximize the NAR signal.

(3) Detailed Description of Improved Magnetic Field Capabilities

We have made quite considerable progress during the past six months in improving our detection capabilities. As discussed elsewhere in this report, one of the greatest challenges in the project is to detect extremely small changes in the magnetic field due to acoustic magnetic resonance. This small magnetic resonance induced change must be distinguished from all of the other time dependent changes in the magnetic field ambient, which could quite easily be orders of magnitude larger than the magnetic resonance induced field changes.

Our approach has been, first, to utilize a very sensitive magnetic resonance based detector, a potassium magnetometer, which, under ideal circumstances, can provide a sensitivity and precision of $1x10^{-13}$ Tesla per root Hertz, and secondly to optimize the sensitivity of this system for our application.

Initial measurements with the potassium system were impossible in a laboratory environment for two reasons; the ambient "magnetic noise" in a laboratory environment is quite large, of order 10^{-7} Tesla at low audio frequency and, perhaps more seriously, the magnetic field gradients in a laboratory environment are also quite large for any exceedingly precise magnetic field measurements.

The performance of exceptionally sensitive magnetometers is inevitably degraded by magnetic field gradients; magnetic resonance based magnetometers are particularly susceptible to field gradients because they measure the local field by monitoring the resonance frequency with a fairly large volume (many cubic centimeters) probe. We wish to measure magnetic field changes of order 10^{-13} Tesla in an ambient of about 10^{-4} Tesla.

So, one would expect parts per billion differences in the field over a sample volume of cubic centimeters would begin to degrade sensitivity at the highest precision levels. This is the case; the GEM Systems people tell us that the precision of the potassium magnetometer begins to degrade with field gradients of tens of nanoTesla/meter.

One of our major goals in the project is a "proof" of concept demonstration that the acoustic magnetic resonance approach can work in a highly idealized environment. Of course, we know that the approach will work in the limit of extremely idealized circumstances, so a second equally important goal is to demonstrate feasibility under circumstances which would plausibly occur outside a highly idealized laboratory apparatus.

We built a nine foot long three layer magnetically shielded chamber and a long solenoid system which generates a highly uniform (tens of nano-Tesla/meter field gradient) which provides an arbitrary magnetic field from 0 to about 0.2 milliTesla. The system is convenient for approximating the earth's field in central Pennsylvania, $0.5x10^{-4}$ Tesla.

This system allows experimental work to be done inside the laboratory, a considerable improvement over our first measurements, carried out in the woods and Penn State golf courses. We've also experimented with a magnetic field gradient minimization system manufactured by Teach Spin Inc. Although we made modest progress in reducing ambient magnetic field gradients with the Teach Spin system, we've made more progress utilizing the shielded chamber/solenoid system. Therefore, this report will summarize results obtained using that system.

As mentioned previously we must develop a system which can detect exceedingly small (~picoTesla or less) changes in the local magnetic field of order 0 .5x10^{-4} Tesla. Background magnetic field "noise" will almost certainly be much greater than the amplitude of our magnetic resonance signal. Therefore, we need to be somewhat clever in developing systems which will, not only provide extremely high sensitivity but which will also simply distinguish between our signal and noise. We are developing several ideas to accomplish this goal.

(a) A Magnetometer "Bridge"

One means to significantly improve signal to noise ratio comes about through the realization that the ambient magnetic field noise comes from fairly distant sources, whereas the signal we wish to measure comes from a very nearby source, our uranium surrogate sample. A simple magnetometer bridge is schematically illustrated in Fig. 3.

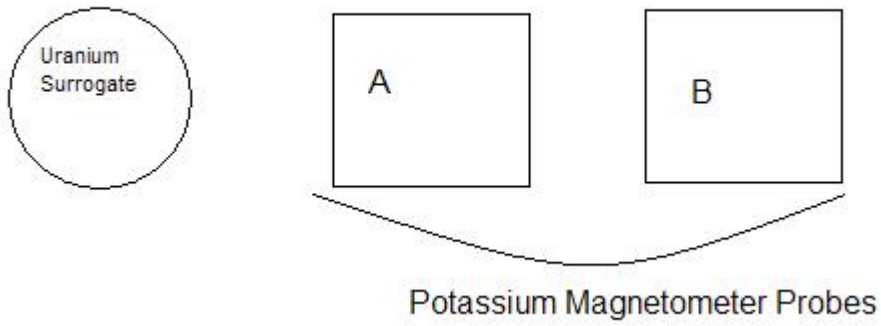

Fig. 3: Simple "bridge" system which utilizes two potassium magnetometer probes, A and B. The magnetic resonance induced changes in the uranium surrogate magnetization will induce local changes in the magnetic field which will be (relatively) much larger at A than at B. However, the background noise will be from much more distant sources and will thus be quite similar at A and B. Therefore, the difference between the magnetic fields at A and B effectively cancels most of the ambient magnetic noise.

Two potassium magnetometers are places in fairly close proximity to one another. One of the magnetometers, Magnetometer A, is placed close to the uranium surrogate. Magnetometer B is considerably more distant. We expect that the two magnetometers will measure quite similar magnetic noise but detect far different responses from the magnetic resonance induced changes in the uranium surrogate sample.

This is the case. Figure 4 illustrates the magnetic field measurements of the potassium magnetometer in the (admittedly idealized) environment of the shielded chamber.

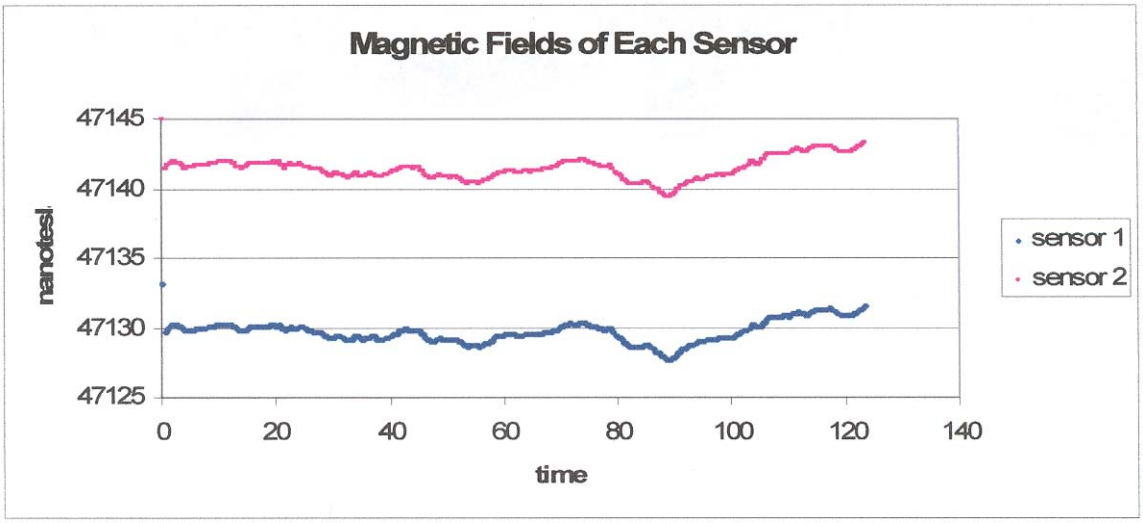

Fig. 4a: The magnetic field noise measured at each of the magnetometer probes. Note that the noise level is about two nanoTesla

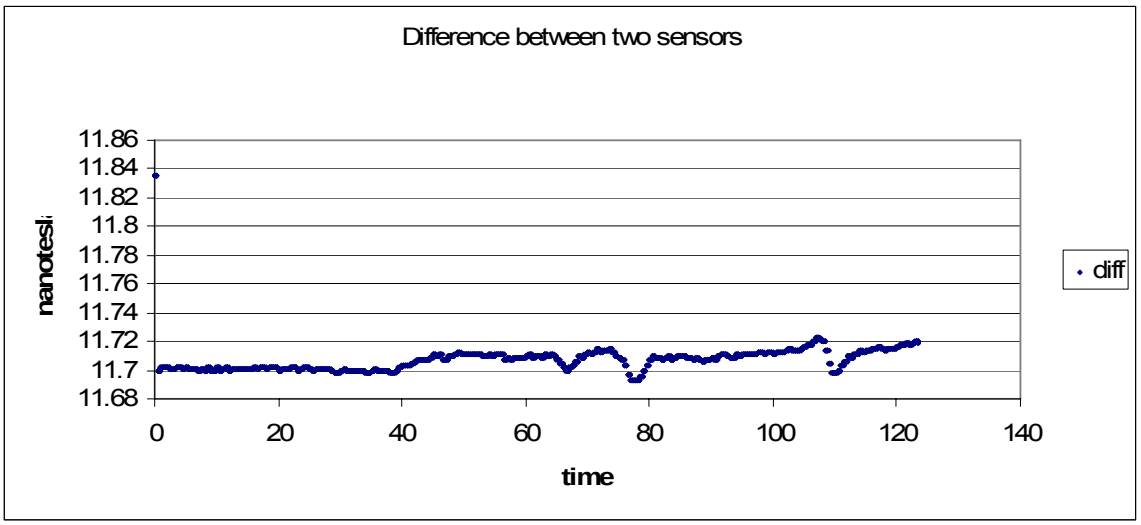

Fig. 4b: The difference between the measurements of the two sensors. Note that the noise level involves occasional spikes of about twenty picoTesla but is largely in the picoTesla range

The local magnetic field noise amplitude is of the order of 2 nanoTesla. However, the difference between probes A and B is much smaller, on average, significantly less than ten picoTesla. Figures 5 and 6 illustrate the advantage of this magnetometer bridge in detection. A single turn coil is placed ~20cm from probe A, of order ~40cm from probe B, a very small periodic waveform generates a magnetic field of about 40 picoTesla at probe A. Although the weak time varying signal is completely lost into the noise of probes A and B, it is clearly visible with a signal to noise ratio of better than 30 to 1 in the real time difference signal determined from the difference between the A and B probe response.

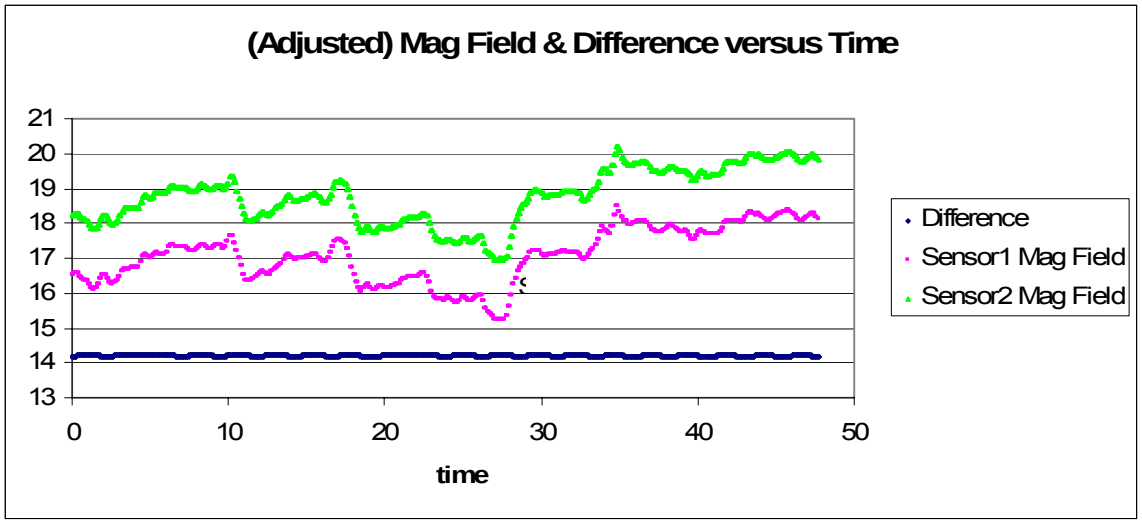

Fig. 5: Trace from the potassium magnetometer probes A and B. (Traces A and B) and a "Bridge" trace the difference between the A and B probe signals.

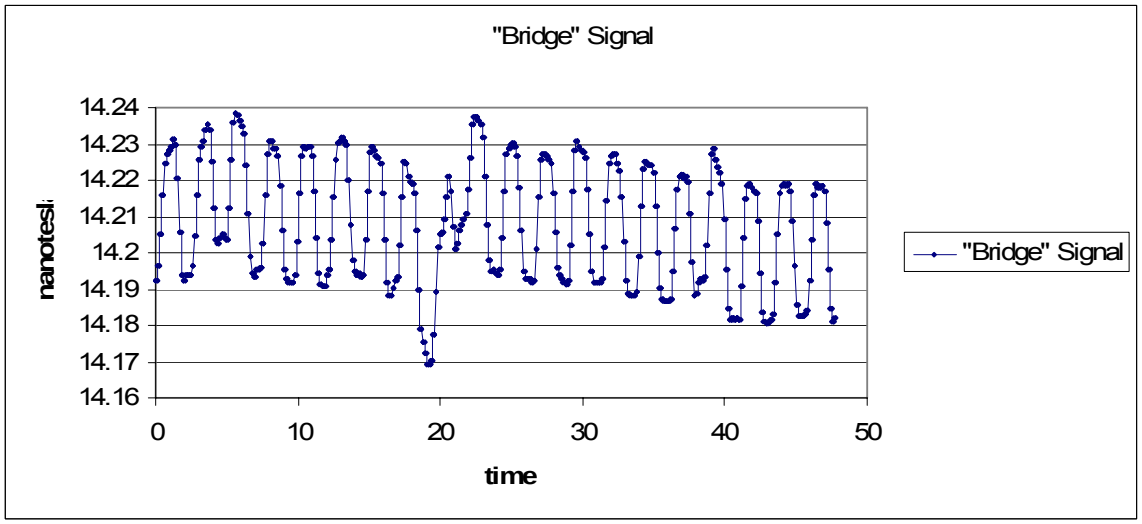

Fig. 6: The bridge probe signal at a higher gain. Note that a ~ 40picoTesla signal appears with a signal to noise ratio of about 30, with the background magnetic field noise level of order a picoTesla, with the occasional large noise spike.. The bridge signal thus allows picoTesla sensitivity in the presence of a background noise level of ~ 2 nanoTesla for an improvement in sensitivity by more than a factor of 1000.

This simple bridge boosts our sensitivity in the presence of a large background by at least a factor of a thousand. Figures 7 and 8 illustrate that an additional easily obtained boost is obtained by repeating a series of 9 measurements of about 23 seconds each. Simple signal averaging, as expected, improves the signal to noise ratio by about the square root of 9 providing a sensitivity of ~3-5x10^{-13} Tesla in a background of ~2x10^{-9} Tesla magnetic noise. An additional (large) improvement in sensitivity is available by utilizing a lock-in amplifier. (The lock-in technique provides phase and frequency sensitive detection.)

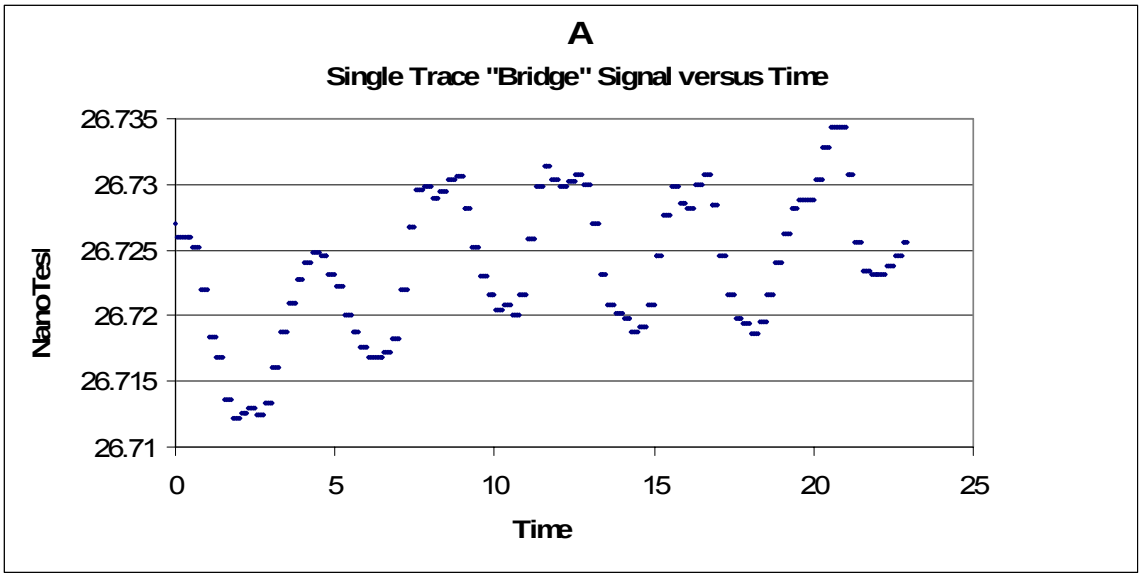

Fig. 7: A single trace with the bridge over a period of ~23 seconds. Note the amplitude of 10 picoTesla.

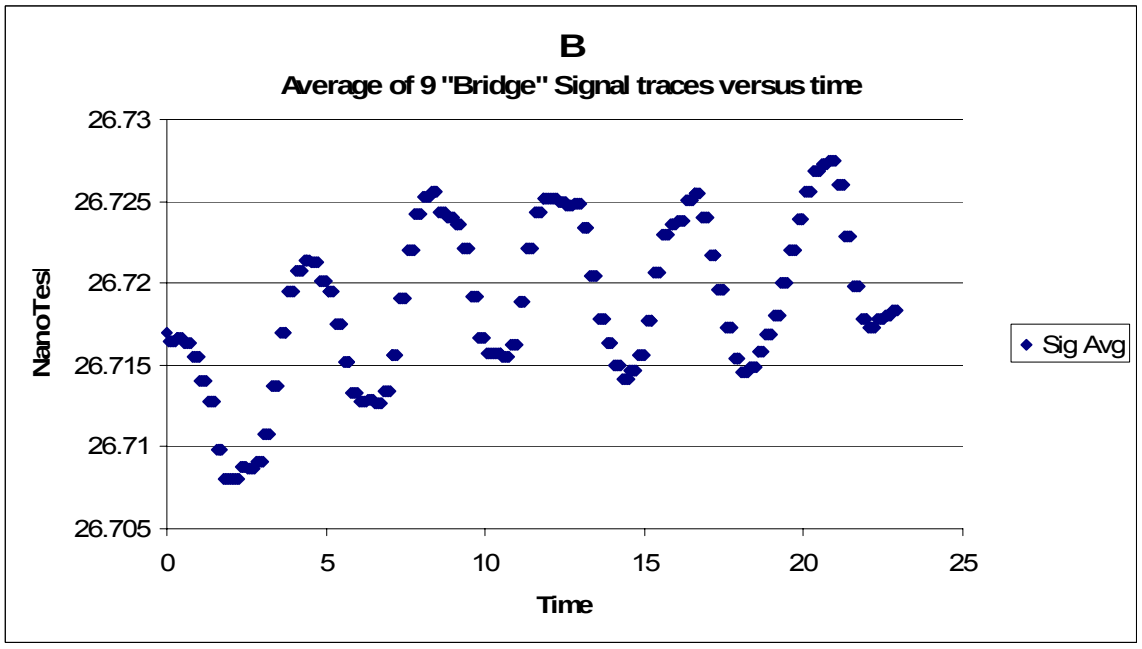

Fig. 8: An average of 9 “bridge” signal versus time. Note the significant improvement from the results of Fig. 4. The signal to noise ratio has improved by about a factor of 3, allowing observations of signal amplitudes of less than 1 picoTesla.

A virtual lock-in amplifier (LIA) was created in Labview software. We’ve evaluated the performance of the LIA in magnetic resonance experiments involving spin dependent recombination (SDR) at fairly low audio frequency (~10^2 Hz) and obtained excellent results compared to a near state of the art commercial system, the Stanford Instrument’s LIA, the SR530. The LIA generates its own modulation/reference signal which eliminates the need for a complex phase lock loop design. Also, the graphical user interface (GUI) associated with Labview virtual instrument (vi) files makes it easy for the user to modify the internal filtering and averaging parameters (see Fig. 9).

The LIA is still in the process of being incorporated into the data acquisition program for the magnetometer. The magnetometer is capable of real time RS-232 data transmission with a maximum baud rate of 115200. We make use of Labview by reading the RS-232 port of the computer and placing the data in an array and processing it in batches. The virtual LIA will add phase and frequency sensitive detection which we believe will lead to a very large additional boost in absolute sensitivity and improve the detection systems ability to discriminate the weak acoustic magnetic resonance signal and ambient noise.

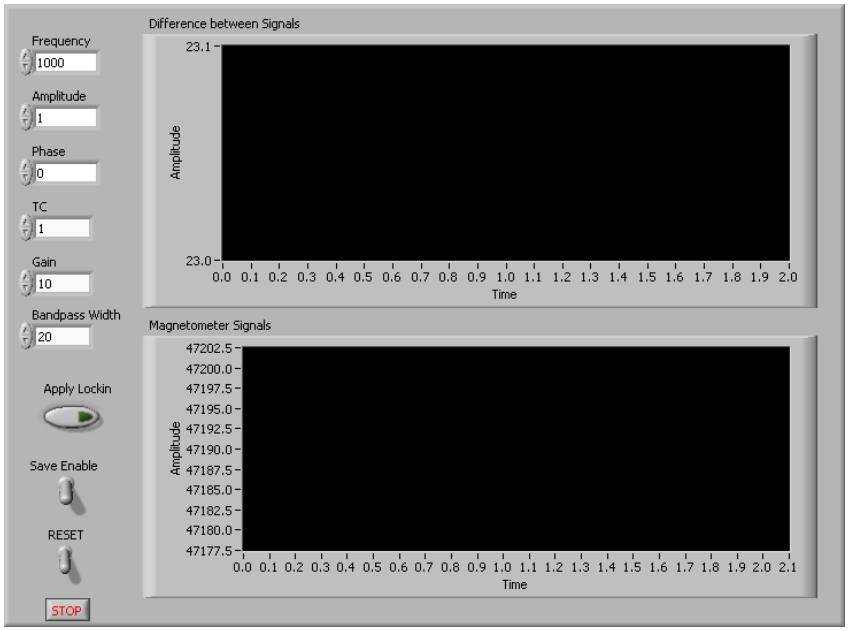

Fig. 9: GUI for the temporary data acquisition/processing system for the magnetometer.

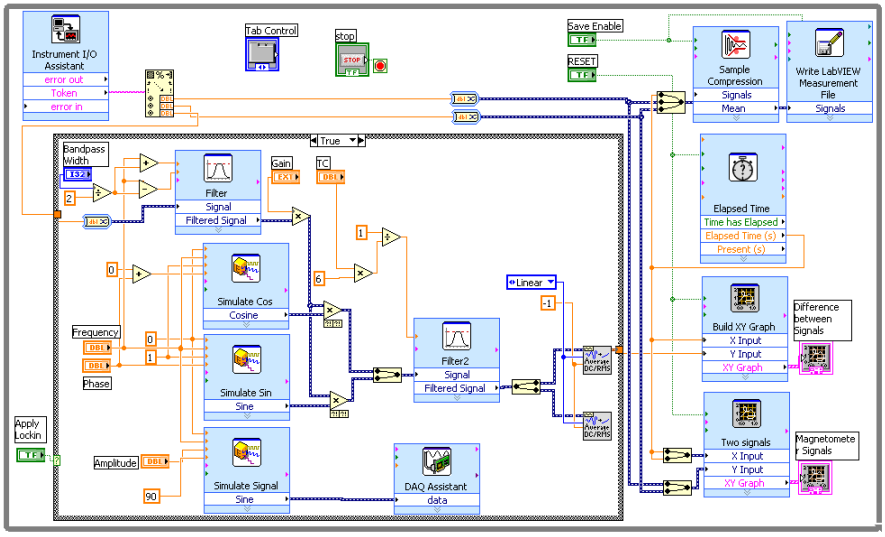

Fig. 10: Block diagram of the temporary data acquisition/processing systems for the magnetometer. This program uses the labview's express vi functions for simplicity.

A schematic of the lock-in program is illustrated in Fig. 10. The system is not quite operational but we anticipate that the addition of the lock-in system will provide a significant additional increase in absolute sensitivity as well as an increased capacity to discriminate between acoustic magnetic resonance signal and ambient noise.

Although funding ended in 2006, we have continued to work on improving the sensitivity of the magnetic resonance detection. With the end of funding, we had achieved a sensitivity of about $3x10^{-13}$ Tesla and were making progress in the development of a low frequency digital lock-in amplifier.

P.M. Lenahan acquired some additional funding to further develop techniques for enhancing the signal to noise ratio of weak magnetic resonance signals. This additional funding allowed C.J. Cochrane and Lenahan to build a digital lock-in, a relatively minor contribution; more importantly, the additional funding allowed them to develop digital signal processing algorithms and hardware utilizing those algorithms which quite significantly enhances the signal to noise ratio of any repeatable slowly varying magnetic resonance signal, such as the weak signal detected with the potassium double resonance bridge system. Cochrane and Lenahan directly demonstrated the improved sensitivity which the hardware and algorithms provide by measuring very weak electrically detected magnetic resonance (EDMR) [1-6] in individual transistors.

The additional sensitivity, still not yet fully optimized, takes the $\sim 3x10^{-13}$ Tesla detection limit below $1x10^{-13}$ Tesla, without even taking into account the additional improvements provided by low frequency lock-in detection. This sensitivity (even without lock-in detection) is available in a measurement span of a few minutes! We believe that the detection sensitivity achieved makes the double acoustic magnetic resonance detection possible and quite possibly practical.

A detailed discussion of digital signal processing techniques which Cochrane and Lenahan developed is discussed below. This work has quite recently been published in the Journal of Magnetic Resonance; see C.J. Cochrane and P.M. Lenahan, J. Magnetic Resonance (2008) doi: 10.1016/j.jmr, 2008.08.004. The work also lead to a patent application; see provisional patent application filing 61/096, 449 "An adaptive signal averaging technique which enhances the sensitivity of continuous wave magnetic resonance and other analytical measurements," Inventors C.J. Cochrane and P.M. Lenahan.

Real Time Exponentially Weighted Recursive Least Squares Adaptive Signal Averaging for Enhancing the Sensitivity of Magnetic Resonance Detection

Cochrane and Lenahan have developed adaptive signal averaging techniques to significantly improve the sensitivity of any magnetic resonance or other analytical measurement in which a repetitively identical or near identical signal is measured at very low signal to noise ratio. In this discussion and demonstration we have utilized digital lock-in amplifier (LIA) detection, though this is not a requirement for the application of the technique. (In the demonstration Cochrane and Lenahan have utilized electrically detected magnetic resonance of small transistors.)

Cochrane and Lenahan developed a way to expedite the averaging process by utilizing the predictability of the autoregressive noise features at the output of the LIA. (The time constant of the LIA determines the correlation between successive samples and

hence, the predictability). We term this tool an adaptive signal averager (ASA) which utilizes adaptive linear prediction as illustrated in figure 1. It works by using the conventional magnetic resonance scan average as the desired response in an adaptive linear prediction configuration. The linear predictor $\boldsymbol{w}_n$ is a finite impulse response (FIR) filter of length p and the input to the linear predictor is the tapped delayed noisy magnetic resonance vector $\boldsymbol{x}(n)$ also of length p, where n is the present time index. These vectors are represented as column vectors which are indicated by the transpose operators T. The input samples $x(n)$ of the vector $\boldsymbol{x}(n)$ are composed of the desired magnetic resonance signal $d(n)$ and an arbitrary noise component $u(n)$.

$$\boldsymbol{w}_n = [w_n(1), w_n(2), \ldots, w_n(p)]^T \tag{1}$$

$$\boldsymbol{x}(n) = [x(n-1), x(n-2), \ldots, x(n-p)]^T \tag{2}$$

The tapped delayed input vector $\boldsymbol{x}(n)$ is analogous to a shift register. First, the vector is initialized to the first p samples of the magnetic resonance signal. Then, when a new sample is acquired, the samples are shifted to make room for the present sample. As a result, the oldest sample is forced out of the input array. This shifting process is then continued until the end of the scan. The present sample of the tapped delayed input vector is represented by the term $x(n\text{-}1)$ which is counterintuitive because this notation implies that it is the first past sample. This notation is used because we are attempting to predict the future sample $d(n)$ based on past values of the noisy input samples $x(n\text{-}1)$ to $x(n\text{-}p)$. This is why this technique is termed linear prediction. The prediction or estimate $d_{est}(n)$ of the desired signal is simply computed by the inner product of these two vectors.

$$d_{est}(n) = \boldsymbol{x}^T(n)\boldsymbol{w}_n \tag{3}$$

The estimate is then subtracted from the scan average to form an instantaneous error $e(n)$ which is used in an algorithm to update the weights of the FIR predictor.

$$e(n) = d(n) - d_{est}(n) \tag{4}$$

There are many forms of adaptive filters but the two most widely used and efficient are the least mean squares (LMS) and recursive least squares (RLS) adaptive filters. These filters are advantageous because they are capable of tracking non-stationary signals and noise and neither algorithm requires an estimate of the signal or noise statistics. This is desired for magnetic resonance experiments because these statistics differ significantly from device to device and vary over time. The main advantage that the RLS algorithm has over the LMS algorithm is that it has about an order of magnitude faster convergence time, though, in most cases, the LMS algorithm is known to have better tracking performance.[7] To increase the tracking performance of the RLS algorithm, Cochrane and Lenahan utilized the exponentially weighted RLS (EWRLS) algorithm by incorporating an exponentially weighing factor λ into the system. By doing this, the algorithm effectively becomes more sensitive to changes in the noise environment. The exponential weighting factor λ controls the memory of the system and is chosen to be in the range $0 < \lambda < 1$. The EWRLS algorithm becomes the RLS algorithm when λ is

chosen to be 1 which provides the system with infinite memory. This implementation is usually undesirable for magnetic resonance measurements with moderate to high SNR because the filtering performance is degraded. This is because the correlation matrix cannot update fast enough when transitioning from noise to signal and vise versa. Therefore, the exponential weighting factor should be kept slightly less than one for signals with moderate to high SNR.

The EWRLS algorithm attempts to minimize the exponentially weighted sum of squared errors cost function which is given by equ. (5).

$$\xi(n) = \sum_{i=0}^{n} \lambda^{n-i} \, | e(n) |^2 \tag{5}$$

In order to minimize this cost function, the gradient is taken with respect to the weights of the FIR predictor and set equal to zero which is given by equ. (6).

$$\nabla\xi(n) = -\sum_{i=0}^{n} \lambda^{n-i} \boldsymbol{x}(i) e(i) = 0 \tag{6}$$

This resultant vector represents the direction of steepest decent on the sum of squared error surface. Plugging in for the error and rearranging yields the set of linear equations given in equ. (7).

$$\left[\sum_{i=0}^{n} \lambda^{n-i} \boldsymbol{x}(i) \boldsymbol{x}^T(i) \right] \boldsymbol{w}_n = \sum_{i=0}^{n} \lambda^{n-i} d(i) \boldsymbol{x}(i) \tag{7}$$

This result can be simplified by realizing that the terms in the brackets on the left is the summation of exponentially weighted deterministic autocorrelation matrices $\boldsymbol{R}_x(n)$ of the input signal from time index $0 < i < n$ and the right hand side is the summation of exponentially weighted deterministic cross correlation vectors $\boldsymbol{r}_{dx}(n)$ of the desired signal and the input signal from time index $0 < i < n$. With this realization, equ. (7) in matrix form is equivalent to equ. (8).

$$\boldsymbol{R}_x(n) \boldsymbol{w}_n = \boldsymbol{r}_{dx}(n) \tag{8}$$

Therefore, the weight vector $\boldsymbol{w}_n$ is found by multiplying the cross correlation vector $\boldsymbol{r}_{dx}(n)$ with the inverse correlation matrix $\boldsymbol{R}_x^{-1}(n)$. Calculation of this inverse is computationally intense so it is not desirable to calculate it every time a new sample is presented to the system. Therefore, one way to reduce the computational time is to realize that $\boldsymbol{R}_x(n)$ and $\boldsymbol{R}_x^{-1}(n)$ can be solved recursively. It can be easily shown that,

$$\boldsymbol{R}_x(n) = \lambda \boldsymbol{R}_x(n-1) + \boldsymbol{x}(n) \boldsymbol{x}^T(n) \tag{9}$$

Now that $\boldsymbol{R}_x(n)$ can be solved for in terms of $\boldsymbol{R}_x(n\text{-}1)$, there needs to be a way to compute the inverse of this matrix. This is called the matrix inversion lemma. The inverse of the

exponentially- weighted autocorrelation matrix in equ. (9) can be solved using Woodbury's identity.[7,8] Woodbury's identity states that matrix A of equ. (10) can be inverted with the relation shown in equ. (11). This identity only holds if A and B are positive-definite p-by-p matrices, D is a positive-definite n-by-p matrix, and C is an p-by-n matrix. The relation is easily shown by computing $AA^{-1} = \mathrm{I}$, where I is the identity matrix.

$$A = B^{-1} + CD^{-1}C^T \tag{10}$$
$$A^{-1} = B - BC(D + C^T BC)^{-1} C^T B \tag{11}$$

Note that the following derivation is for real valued data. The transpose operations would be replaced with the hermitian operator for imaginary valued data. Comparing equ. (10) and (11), it can be realized that

$$A = \boldsymbol{R}_x(n) \tag{12}$$
$$B^{-1} = \lambda \boldsymbol{R}_x(n-1) \tag{13}$$
$$C = \boldsymbol{x}(n) \tag{14}$$
$$D = 1 \tag{15}$$

Then, plugging equ. (12) - (15) into (11), the exponentially weighted inverse autocorrelation matrix can be computed recursively as follows.

$$\boldsymbol{R}_x^{-1}(n) = \lambda^{-1}\boldsymbol{R}_x^{-1}(n-1) + \frac{\lambda^{-2}\boldsymbol{R}_x^{-1}(n-1)\boldsymbol{x}(n)\boldsymbol{x}^T(n)\boldsymbol{R}_x^{-1}(n-1)}{1 + \lambda^{-1}\boldsymbol{x}^T(n)\boldsymbol{R}_x^{-1}(n-1)\boldsymbol{x}(n)} \tag{16}$$

This equation is usually reduced into simpler form, as shown in equ. (17)

$$\boldsymbol{R}_x^{-1}(n) = \frac{1}{\lambda}\left[\boldsymbol{R}_x^{-1}(n-1) - \boldsymbol{g}(n)\boldsymbol{z}^T(n)\right] \tag{17}$$

where,

$$\boldsymbol{z}(n) = \boldsymbol{R}_x^{-1}(n-1)\boldsymbol{x}(n) \tag{18}$$
$$\boldsymbol{g}(n) = \frac{1}{\lambda + \boldsymbol{x}^T(n)\boldsymbol{z}(n)}\boldsymbol{z}(n) = \boldsymbol{R}_x^{-1}(n)\boldsymbol{x}(n) \tag{19}$$

The next step is to solve for the weight update. As stated earlier, the weight vector is found by multiplying the cross correlation vector $\boldsymbol{r}_{dx}(n)$ with the inverse correlation matrix $\boldsymbol{R}_x^{-1}(n)$. To reduce computation, $\boldsymbol{r}_{dx}(n)$ is solved recursively in a similar fashion to that of $\boldsymbol{R}_x(n)$ and is shown below.

$$\boldsymbol{r}_{dx}(n) = \lambda \boldsymbol{r}_{dx}(n-1) + d(n)\boldsymbol{x}(n) \tag{20}$$

The weight vector is found by computing the product of the autocorrelation matrix $\boldsymbol{R}_x^{-1}(n)$ obtained in equ. (16) and the recursive cross correlation vector $\boldsymbol{r}_{dx}(n)$ formed by equ. (21) and realizing that $\boldsymbol{R}_x^{-1}(n-1)\boldsymbol{w}_{n-1} = \boldsymbol{r}_{dx}(n-1)$.

$$\boldsymbol{w}_n = \boldsymbol{R}_x^{-1}(n)\boldsymbol{r}_{dx}(n) = \boldsymbol{w}_{n-1} + \boldsymbol{g}(n)\alpha(n) \tag{21}$$

where $\boldsymbol{g}(n)$ was defined previously and $\alpha(n)$ is the a priori error. The priori error is the error that occurs when using the previous set of filter coefficients $\boldsymbol{w}_n$ and is shown below,

$$\alpha(n) = d(n) - \boldsymbol{x}^T(n)\boldsymbol{w}_{n-1} \tag{22}$$

It is easy to see that the computation has been reduced significantly from the conventional LS algorithm because of the recursive nature of the autocorrelation and cross correlation functions. $\boldsymbol{R}_x^{-1}(n)$ can be initialized directly or by forming the matrix $\delta \cdot \mathbf{I}$, where δ is a constant called the regularization parameter and $\mathbf{I}$ is the identity matrix. The initialization of δ depends on the SNR of the signal under observation and should be calculated with the following[7,11]

$$\delta = \sigma_u^2(1-\lambda)^{\alpha} \tag{23}$$

where σ_u^2 represents the noise variance of an individual magnetic resonance scan, λ is the exponential weighting factor, and α is a constant to be determined by the SNR of the magnetic resonance scan. The parameter α should be chosen to be 1 for SNR > 30 dB, $-1 < \alpha < 0$ for SNR ~ 10 dB, $\alpha < -1$ for SNR < -10 dB.[7,11]

In some cases, the RLS algorithm can become unstable due to its mathematical formulation. This occurs when the inverse autocorrelation matrix loses its symmetry property.[7,9] This can be avoided simply by calculating the lower (or upper) triangle of the inverse autocorrelation matrix and filling the upper (or lower) triangle to preserve its symmetry property.[7,10] This technique is attractive not only because it prevents instability, but it also reduces computation. We utilized this method because we initially encountered instability problems.

As mentioned earlier, the ASA filters each incoming magnetic resonance scan in real time via the EWRLS algorithm. The conventional average is used as the desired signal in the algorithm and can be thought of as an approximate guide for the filter to follow. Therefore, the filter allows the noise that it sees to pass, but it effectively reduces the variance of it thereby acting as a low pass filter with a time constant proportional to $(1-\lambda)^{-1}$.[7] It is important to note that even though this adaptive filter may have a similar Fourier transform compared to that of a conventional low pass filter, it differs in many ways. A conventional low pass filter simply does not allow the input signal to pass any frequency greater than the cutoff frequency of the filter. The adaptive filter also acts as a frequency blocker but differs from a low pass filter because its weights are adapted so as to minimize the error between the desired signal and its prediction. As result, adaptive

filters are capable of limiting the variance of the input signal relative to the desired signal. The filter only allows the variance of the input signal to deviate from the desired signal within a certain threshold. This is precisely why adaptive filters have superior performance to that of conventional low pass filters.

This filter is ideal for magnetic resonance experiments because one usually sacrifices a smaller time constant for the observation of noisier signals. As a result, each individual spectrum will contain more noise and will require the need for longer signal averaging to obtain a reasonable SNR. The filtered output scans are then averaged separately. The underlying idea for this action is that because the noise of the filtered scans is reduced, the noise in the filtered average will be reduced faster than that of the noise in the conventional average.

In conventional signal averaging, assuming the noise has a Gaussian distribution and is independent and identically distributed (iid) with variance σ_u^2, the averaged noise variance σ_{uN}^2 is reduced by a factor of the number of scans N in the average as given in equ. (14).

$$\sigma_{uN}^{\ 2} = \frac{\sigma_u^{\ 2}}{N} \tag{24}$$

The reduction in noise of the ASA can be determined by analyzing the error that is introduced into the algorithm. For an individual scan, the error introduced into the system by the filter is the combination of the averaged noise in the conventional average $u_N(n)$ with variance σ_{uN}^2 and the prediction error of the filter $v(n)$.

$$e(n) = d(n) - d_{est}(n) = \left[d(n) + u_N(n)\right] - \left[d(n) + v(n)\right] = u_N(n) - v(n) \tag{25}$$

For ease of analysis, it is assumed that the prediction error is also Gaussian random variable and has 0 mean and variance σ_v^2. Therefore, the variance of the error σ_e^2 for an individual scan is found by adding the variances of each of the random variables.

$$\sigma_e^{\ 2} = \sigma_{uN}^{\ 2} + \sigma_\upsilon^{\ 2} = \frac{\sigma_u^{\ 2}}{N} + \sigma_\upsilon^{\ 2} \tag{26}$$

If M filtered scans are averaged, then the reduction in noise variance achieved by the ASA is simply given in equ. (17).

$$\sigma_{e_M}^{\ 2} = \frac{\sigma_u^{\ 2}}{NM} + \frac{\sigma_\upsilon^{\ 2}}{M} \tag{27}$$

where $M < N$. The reason M scans are averaged and not N is because we want the conventional average to build up a reasonable desired response before the filter is applied so a better prediction can be achieved. N is not that much greater than M so they are approximately equal when considering longer averages. Therefore, as N and M get larger, the faster the first term in (17) dies away which implies that the dominating source of

noise will eventually be due only to the prediction error of the filter. This is desirable because it is this first term that actually slightly biases the ASA. By allowing the conventional average to build a reasonable desired signal before the filter is applied, the noise bias is gradually removed. It turns out that not many scans are required to be averaged for this bias to be removed.

Another concern one might have would be whether or not the adaptive filter would have any effect on the measurements precision. Does the process itself introduce some systematic error? On e way to test for this is to compare measurements of the zero crossing g value of an electrically detected magnetic resonance measurement in which standard signal averaging and the adaptive technique are utilized. . It turns out that this technique does not introduce any significant shift in the spectrum, which would be expressed in a shift in the g value. The reason for this is because an FIR filter of small length (< 256 weights) is used in our implementation. FIR filters have a linear phase and introduce a small constant delay at the output of the filter. This delay is actually filter length dependent so that longer delays are encountered for filters of longer length. Though, this delay for longer length filters is not significant enough to introduce any significant error in the measurement. This was confirmed when a relatively long filter (1024 weights) was used in the algorithm to find the g value of a particular electrically detected magnetic resonance signal. The g values from the unconventional average differed from the filtered average by about 0.000001. One usually reports g values with a much larger margin of error of ± 0.0003. Therefore, the small error introduced by the filter is negligible.

As discussed earlier, the prediction of the desired signal is always better than or equal to that of the noisy input because the filter is optimized to minimize the sum of squared errors. Therefore, the reduction in noise of the filtered average will always be better than that of the original average over time, despite being averaged with fewer scans. As a result, one can see why this averaging process is expedited; averaging a random variable with a small variance (prediction error) will converge much faster than averaging a random variable with larger variance (noise error).

The EWRLS ASA was implemented in Labview version 8.2 software. Since the completed double acoustic magnetic resonance system was not yet available, the technique was applied to electrically detected magnetic resonance for a MOSFET. This measurement, like the double acoustic magnetic resonance measurement, also involves a slowly varying and repeatable magnetic resonance response. The spectrometer settings used in the scans were purposely chosen to reduce the SNR of the signal so as to better visually observe the improvement of the filtered signal. The variables that were used in the EWRLS algorithm were $\lambda = 0.98$, $\delta = 1$, $p = 32$ weights, and the filter was applied after averaging 15 scans. The reason 15 scans were averaged before the filter was applied was so that the filter had a better represented spectrum (moderate SNR as opposed to low SNR) upon which to base its prediction. Also, 15 scans in the conventional average were enough to remove the noise bias which was discussed previously.

Figure 2 compares the performance of the filter of an individual scan. With the signal amplitude normalize to 1, the noise variance was calculated to be $\sigma_u^2 = 0.0315$ in the unfiltered trace and was calculated to be $\sigma_u^2 = 0.00278$ for the filtered trace. (These values were calculated by taking the variance of the difference between the individual scan and the final average.) As a result, an 11.3 times reduction in noise variance was

observed in a single scan which corresponds to a 11.3 times reduction in time as well. Figure 3 compares the average of 100 unfiltered scans and the average of 85 filtered scans. Note that the filtered average isn't as noisy as the conventional average and has almost converged to its final value. Figure 4 compares the average of 1000 unfiltered scans and the average of 985 filtered scans. Note that significant noise is present in the unfiltered average whereas the noise is not visually observable in the filtered average. Also, the variance of the noise that remains in the conventional average after 1000 scans is approximately equal to the noise variance in the filtered average after about 90 or so scans as illustrated in figure 5. As a result, the reduction in a noise variance by factor of 11.3 in an individual scan is equivalent to a reduction in time by the same amount as illustrated in figure 6. In this particular experiment, the conventional average (1000 scans at 1 minute each) took 1000 minutes to complete. The filtered average converged in approximately 90 scans which amounts to 910 less minutes of scanning time to obtain a comparable SNR. This is a very significant consideration, especially for measurements that require days of signal averaging. A signal that would usually require 10 days of signal averaging would be reduced to averaging for less than 1 day (assuming similar filter performance).

A concern one might have would be when to apply the filter. It turns out, that even if the SNR is less than 1, the filtered average will converge to the same result as the original average. This is ok to do so long as a sufficient number of scans are averaged first before the filter is applied to remove much of the noise bias, as discussed earlier. Cochrane and Lenahan applied the ASA to another transistor which has a magnetic resonance spectrum which has weak side peaks due to hyperfine interactions with nearby ^{13}C and ^{29}Si. This hyperfine structure is unobservable until at least 20 or so scans in the average. The filter was applied after 15 scans (before any of the weak hyperfine structure was observed) and our results show that the unfiltered average and the filtered average are identical after 250 scans. The only difference is that the filtered average converged in many fewer scans.

The EWRLS ASA is ideally suited for the proposed low field double acoustic magnetic resonance detection measurements. It is also an extremely useful and efficient tool for any continuous wave magnetic resonance measurement. It is capable of reducing the noise variance by a factor of 11.3 in a single trace and as expected, the average of the filtered scans was shown to converge by a similar factor. This filter is even successful when the SNR of a magnetic resonance scan is less than 1. With such great reduction in noise, the ASA effectively expedites the time of averaging. In addition to low field double acoustic magnetic resonance, this tool has great potential for magnetic resonance in general. One other example of particular importance: this approach may be very useful in quantum computing experiments where extensive signal averaging may be required for single spin detection. This filter can also be applied to any field where extremely high sensitive and relatively short acquisition times are required. Furthermore, it should be noted that this filter can also be applied to any field where signal averaging is utilized.

REFERENCES

[1] D.J. Lepine, Phys. Rev. B **6**, 436 (1972).
[2] D. Kaplan, I. Solomon, and N. F. Mott, Civ. Eng. Mag. **39**, L51 (1978)
[3] J.P. Campbell, P.M. Lenahan, C.J. Cochrane, A.T. Krishnan, S. Krishnan, *IEEE Trans. on Dev. and Mat. Rel*., Volume 7, Issue 4, pp. 540 - 557, Dec. 2007 .
[4] C.J. Cochrane, P.M. Lenahan, A.J. Lelis, *Appl. Phys. Lett.* 90, 123501 (2007).
[5] J.A. Weil, J.R. Bolton, and J.E. Wertz, *Electron Paramagnetic Resonance: Elementary Theory and Practical Applications*. John Wiley and Sons Inc., New York, NY, 1994.
[6] Aldert van der Ziel, *Noise in Solid State Devices and Circuits*, Wiley, (1986).
[7] P.D. Petrova, *TELSIKS*, vol. 2, pp. 577-580, (2003).
[8] S. Pajevic, G. H. Weiss, K. W. Fishbein, and R. G.S. Spencer, Use of the Adaptive Line Enhancement Filter for SNR Improvement in NMR Spectroscopy, Proc. Intl. Sot. Mag. Reson. Med. 8 (2000) 1778.
[9] S. Haykin, Adaptive Filter Theory, 4th edition, Prentice Hall, Inc., (2002).
[10] M. Hayes, Statistical Digital Signal Processing and Modeling, John Wiley & Sons, Inc., (1996).
[11] M.H. Verhaegen, Automatica, Vol. 25, No. 3, pp. 437-444, 1989.
[12] B. Yang, IEEE Trans. Sig. Proc., Vol. 42, No. 12, Dec. 1994.
[13] G.V. Moustakides, *IEEE Trans. on Sig. Proc.* **45** (10): 2468-2476, Oct. (1997).

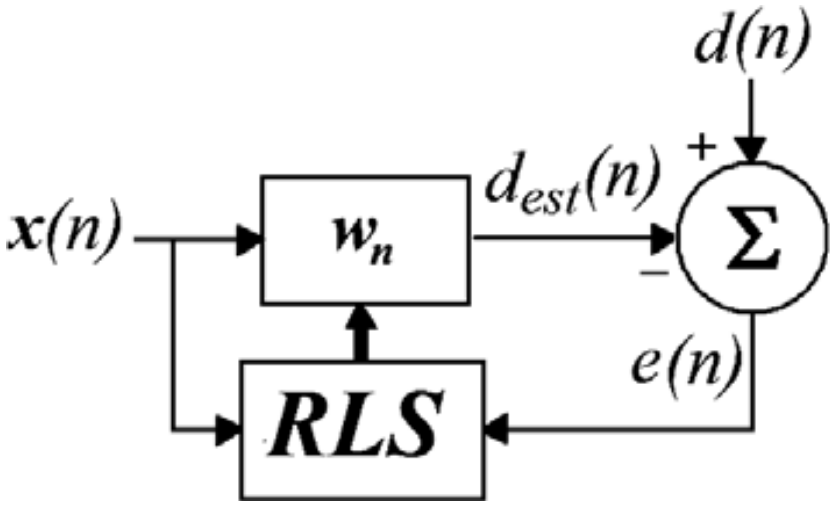

Figure 1: Block diagram of the adaptive linear predictor using the EWRLS algorithm. $\boldsymbol{x}(n)$ represents the input vector composed of samples $x(n\text{-}1)$ to $x(n\text{-}p)$ and $\boldsymbol{w}_n$ represents the FIR predictor of length p. The predictor output $d_{est}(n)$ is subtracted from the desired signal $d(n)$ (the conventional average) to form an instantaneous error $e(n)$. This error, along with the input vector, is fed into the RLS algorithm to update the weights of the filter so that a better prediction can occur when the next sample is presented to the system.

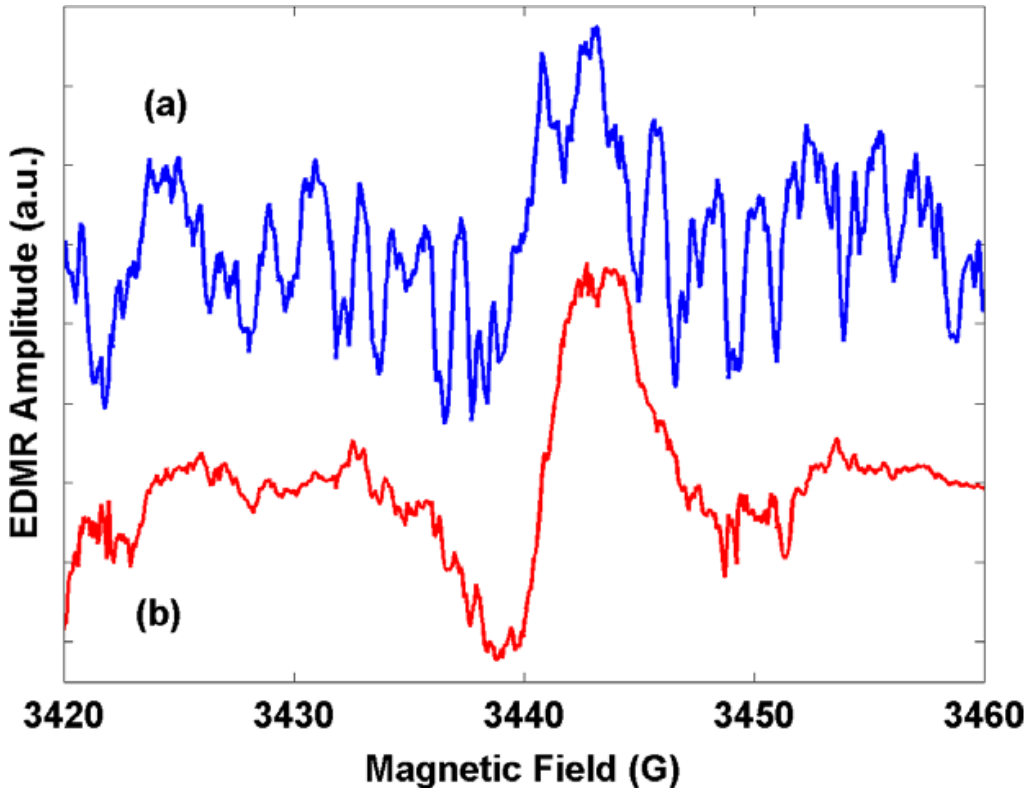

Figure 2: Individual unfiltered scan (a) compared to the individual filtered scan (b).

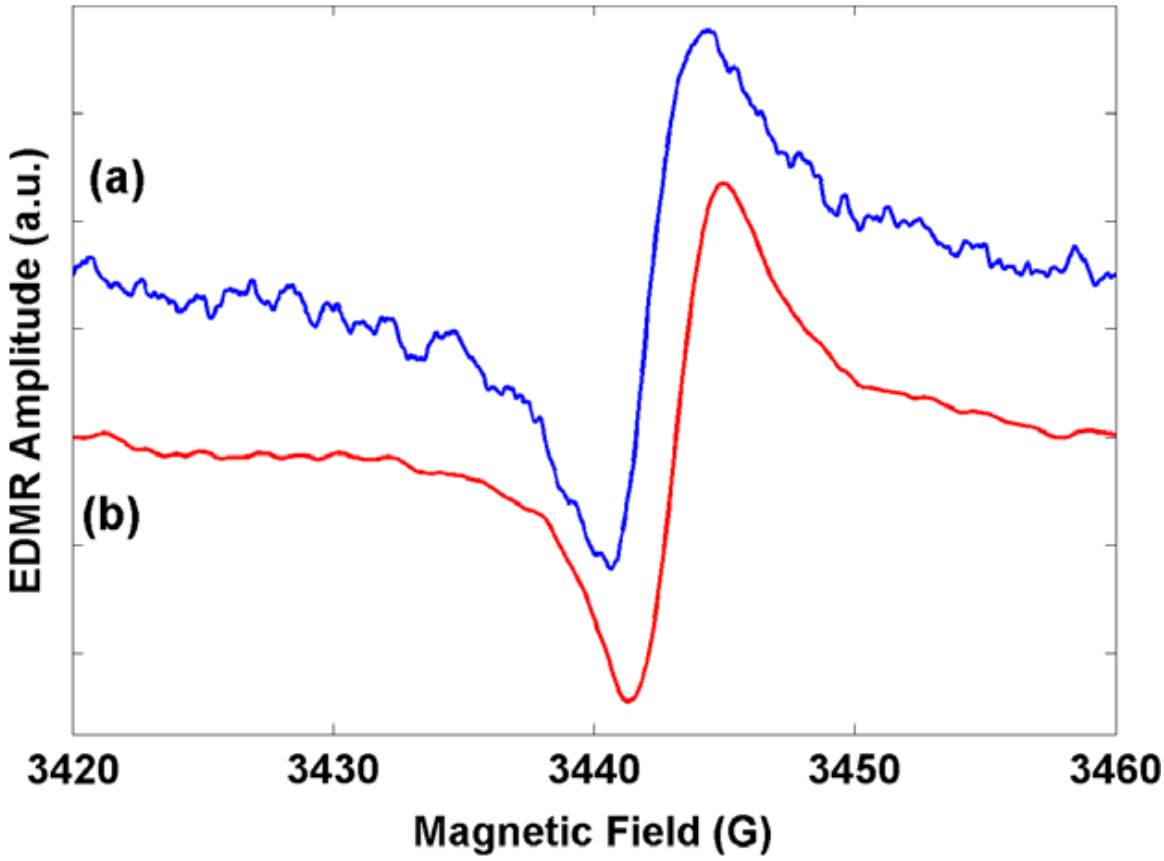

Figure 3: Average of 100 unfiltered scans (a) compared to the average of 85 filtered scans (b).

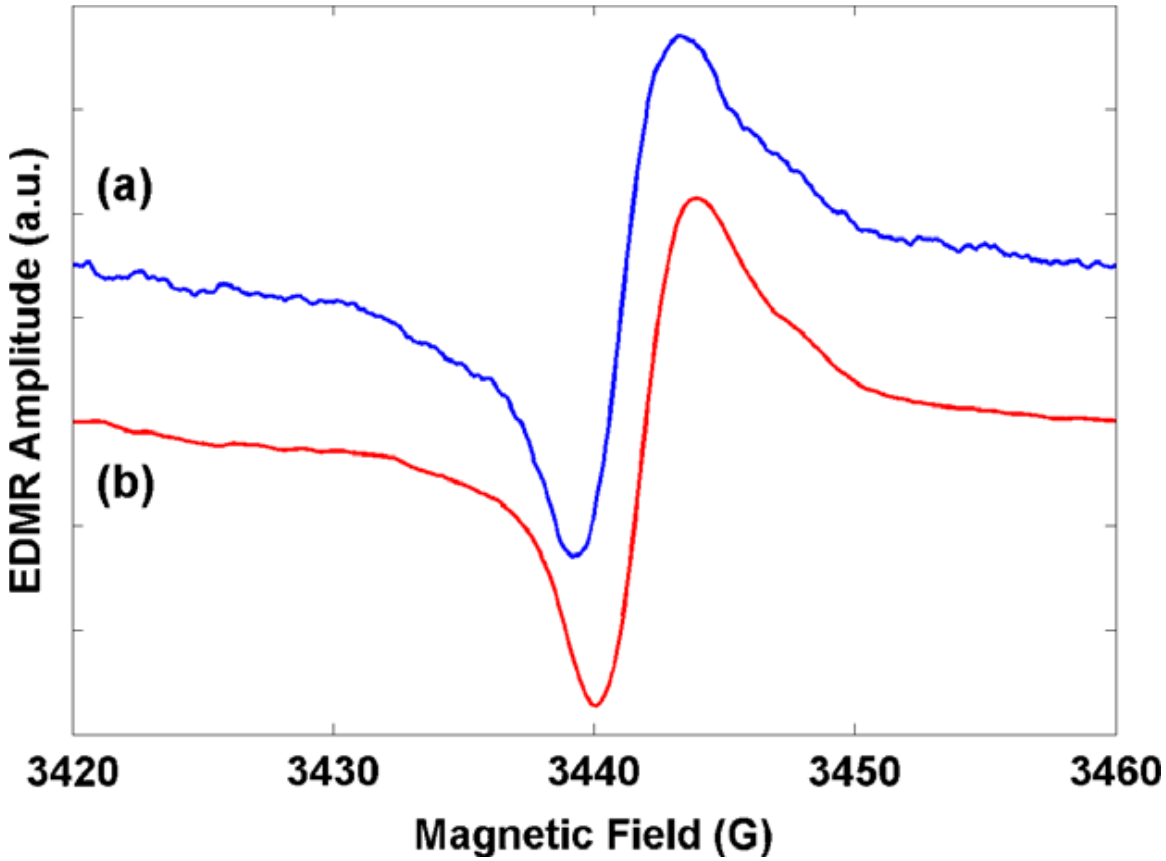

Figure 4: Average of 1000 unfiltered scans (a) compared to the average of 985 filtered scans (b).

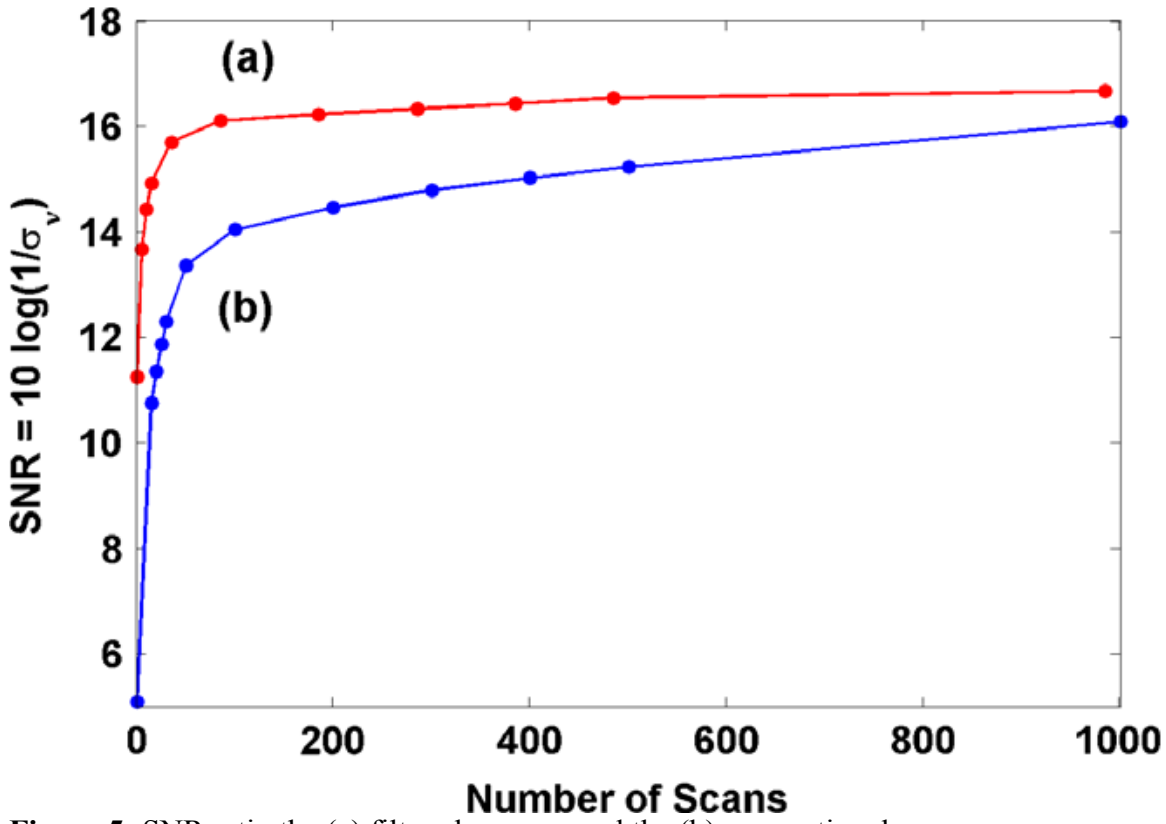

Figure 5: SNR ratio the (a) filtered average and the (b) conventional average.

Status of Acoustic Studies

(1) Technical Approach

The primary objective of this part of the project is to interrogate non-intrusively the target material in a closed air-filled container. To that end, the power of ultrasound is to be used to excite the nuclear and electron spins of the target material, to achieve the respective resonances. However, it is common knowledge that sound, especially in the ultrasonic frequency regime, attenuates rather drastically when traveling through air. Therefore, the idea of pressurizing the chamber that contains the target material was put forth, as air when pressurized, has a lower attenuation than at atmospheric pressure.

Theoretical calculations were made to determine the nuclear and electron spin resonance frequencies of the surrogate material Aluminum, at earth's magnetic field (0.5 x 10^{-4} Tesla). They are 599.57 Hz and 1.511 MHz respectively. Ultrasonic PZT stack transducers were acquired to impart acoustic energy at the required frequencies to the Aluminum specimen. Power amplifiers were used to increase the amount of acoustic strain imparted to the specimen. A Laser Doppler Vibrometer (LDV) was utilized to obtain measurements of strain in the Al specimen.

The Polytec® OFV-505 laser doppler vibrometer is a very sensitive displacement measuring device capable of observing displacements in the ranges of few nanometers. The frequency of operation is up to 1.5 MHz. However, with the addition to the current LDV set up, the sensitivity is can go much higher thereby enabling us to accurately monitor the absorption of acoustic energy by the Aluminum specimen. The new set up is

able to measure displacements less than a picometer (< 10^{-12} m). This corresponds to, in a 10 cm long specimen, an ability of monitoring strains of the order of 10^{-10}. The frequency range of operation of the LDV is can go higher as well (~ 30 MHz). The ability to work at higher frequencies enables us to work with shorter specimens, which in turn, aids us in achieving higher Q factors.

When acoustic waves are transmitted into the specimen and at the nuclear resonance frequency, there is absorption of energy by the nuclear spin system. The laser doppler vibrometer (LDV) would be monitoring the vibration of the specimen as the frequency sweep is conducted. There is an inherent loss of acoustic energy (attenuation) during the vibration of the specimen. However, when the nuclear resonance frequency is reached, there can be further loss of energy (more attenuation). By continuously monitoring the attenuation using the LDV, we can observe the nuclear acoustic resonance in Aluminum and other specimens. It has been shown in the past that nuclear acoustic resonance could be observed by monitoring the absorption of the incident acoustic energy at resonance. We intend to proceed on a similar path, however, utilizing the laser doppler vibrometer to observe the attenuation of the incident sound wave. This is the first time ever when a laser doppler vibrometer is used to observe nuclear acoustic resonance.

It has been shown in literature that nuclear acoustic resonance can be observed by monitoring the nuclear spin-phonon absorption coefficient. When acoustic waves are transmitted into the specimen, there is absorption of energy by the nuclear spin system at the nuclear resonance frequency. LDV can be monitoring the vibration of the specimen during the frequency sweep. There is an inherent attenuation of transmitted acoustic energy due to the specimen vibration, however, when the NAR frequency is reached, there can be a sudden increase in attenuation. By continuously monitoring the attenuation using the LDV, we can be able to observe NAR in Aluminum and other specimens.

Initial experiments were performed to determine the Quality factor (Q-factor) of ultrasound transmission using the PZT stacks into the Al specimen at frequencies of concern to us. Although the numbers were low, efforts were made to modify the experimental set up, such as the specimen holder, to increase the Q-factor. Radial displacement distributions in the specimen were also measured using the LDV to understand the extent of uniformity of displacements throughout the specimen. These results were then compared with simulations and the correlation was satisfactory.

A pressure vessel/chamber that could withstand pressures up to 2000 psi was designed and fabricated to aid us in air-coupled ultrasonic transmission of energy into the target specimen (see Fig. 11). This is a very significant step in the whole exercise as this provides us with a method to interrogate the target material non-intrusively. The pressure vessel was incorporated with a small Plexiglas window so that LDV could be used to perform NAR measurements..

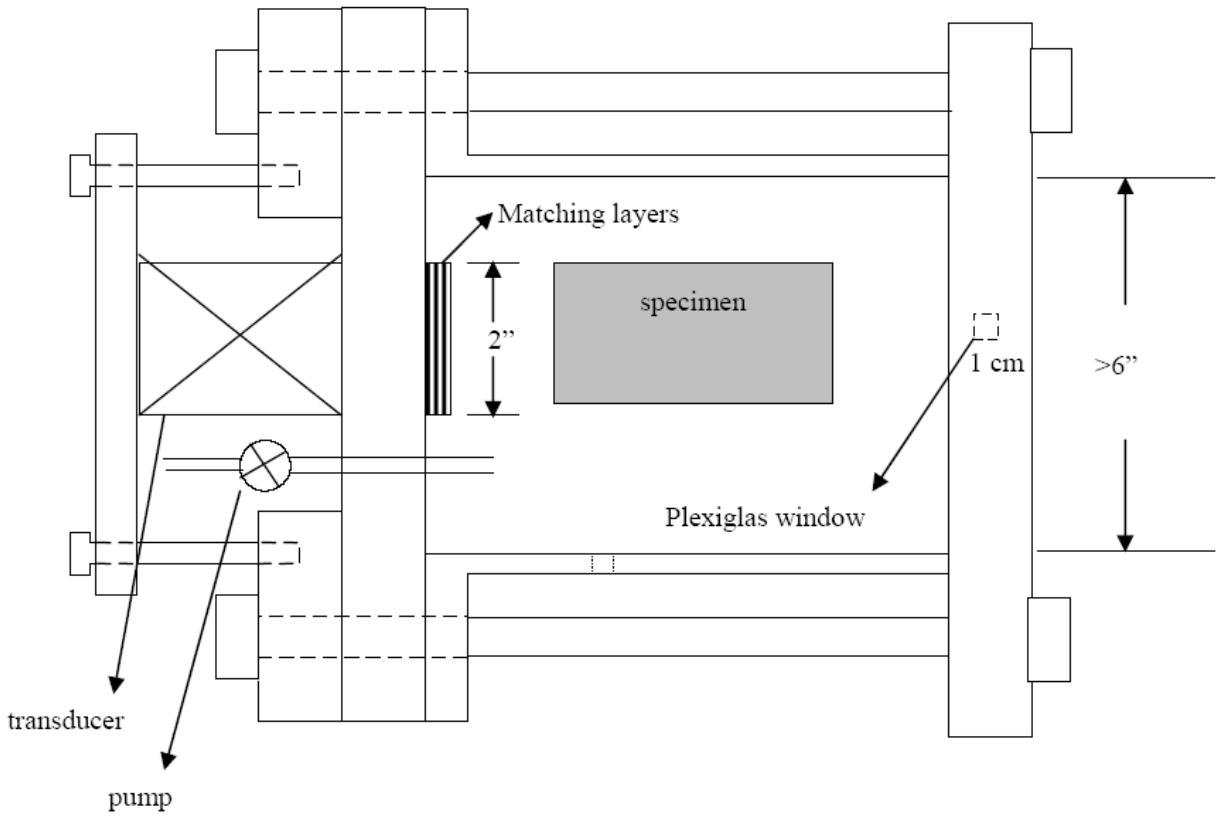

Figure 11(a). The fabricated Pressure Vessel to facilitate air-couple ultrasound transmission showing the transducer outside the chamber, matching layers, specimen inside the chamber and also the Plexiglas window for LDV measurements

The first series of tests involved the measurement of displacements in the Al specimen using the LDV while sound is transmitted into the chamber by PZT stacks attached to the outside of it. Matching layers made of cork were used to reduce losses due to the mismatch of acoustic impedances from the transducer stack to the transmission media.

There are many different aspects of the pressure vessel setup that need to be determined before the NAR tests could be performed efficiently with good understanding. The frequency characteristics of all the individual components of the acoustic transmission line have to be understood clearly. However, performing experiments to comprehend the effects of all these variables is time consuming. Therefore, Finite Element Modeling of the experimental set up to simulate the displacements generated in the Al specimen was begun.

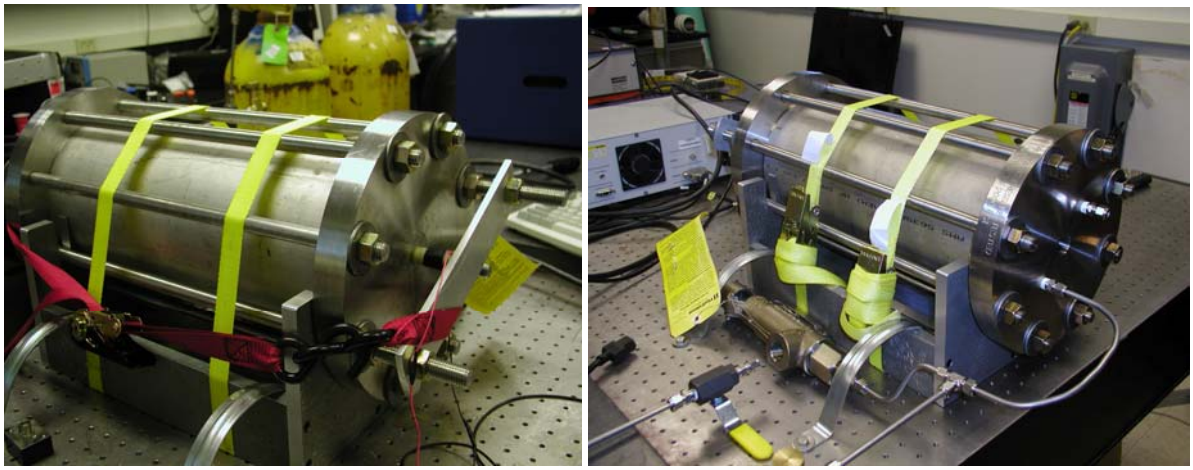

Fig. 11(b): The fabricated pressure vessel to facilitate air-couple ultrasound transmission, Note the modifications made at each end.

Coupled Acoustic-Piezoelectric Analysis (CAPA) is a powerful solver of Finite Element models constructed using ANSYS for acoustic energy transmission models. The different parameters that have been studied so far, using CAPA are:

1. The effect of matching layer thickness on the transmission of ultrasound into the pressure vessel, and its dependence on frequency.
2. The effect of the thickness of the end-cap of the pressure vessel: This was done to explore the idea of not using matching layers and instead use the correct thickness of the end-cap to maximize the transmission of acoustic energy into the target specimen.
3. The effect of the pressure inside the vessel on the displacements induced in the Al specimen.
4. The overall frequency characteristics of the entire experimental set-up.

(2) Results

Experiments have been conducted already to determine the efficacy of using a Finite Element model to simulate the air-coupled transmission of ultrasound at higher pressures. The initial results are very encouraging as there is sufficient matching between experiments and simulations. However, the model itself needs to be further refined in terms of incorporating experimental conditions such as three-point specimen holder etc. Currently, a two-dimensional, axi-symmetric model (see Fig. 12) was constructed and solved to provide initial ideas about the behavior of the entire system, but for future simulations, a three-dimensional model will be constructed to accurately simulate the experimental set up.

The finite element model utilized here has an element rate of 20 per wavelength. The component in the system with the least wavelength would be utilized for spatial discretization of the components. In this case, it is the cork matching layer.

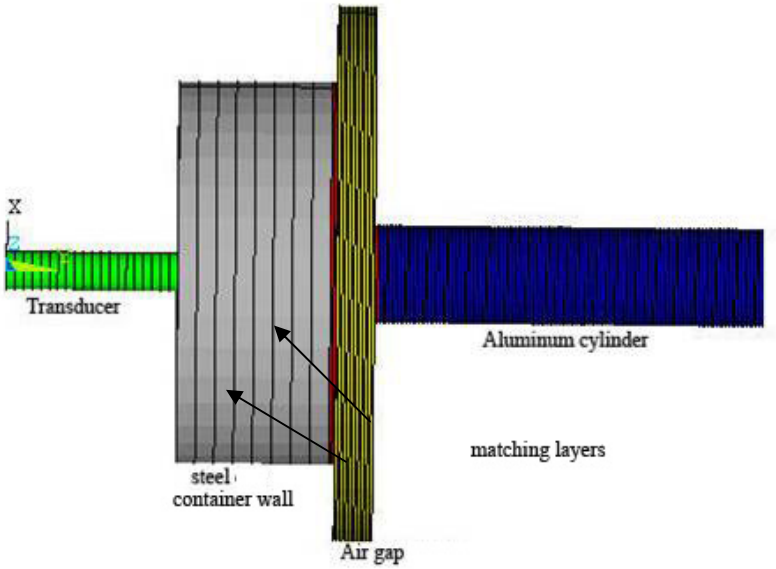

Fig. 12: ANSYS Model setup

The different materials and the corresponding material parameters utilized in the model are provided in the Table 1.

Table 1: Material Properties

Material	Thickness (mm)	Velocity (m/s)	Density (kg/m3)	Acoustic Impedance (MRayls)
PZT-5A	44.75	3951	7750.25	30.62
Steel	40	5913	7847	46.39
“Quiet” Cork	0.8–1.5	500	240	0.12
Air	10	343	1.205	0.000413
Aluminum	100	6318	2700	17.06

(a) Frequency Component Analysis

As the first step in the simulation of the set up, transient analysis of the model was performed to understand the frequency components that might arise from this rather complicated system (see Fig. 13). This involves the use of a broadband acoustic pulse to be applied to the transducer and transmit energy in to the system and observe the system’s response in terms of the acoustic displacements generated in the Aluminum cylinder located inside the container. Calculations were carried out to estimate the structural resonant frequency of every component of the system, namely, transducer, container wall, matching layer, air gap and the Aluminum cylinder, based on their thicknesses and the velocity of sound in them. They are, 32 kHz, 73.9 kHz, 156 kHz, 17 kHz and 32 kHz, respectively. The result from the simulation when analyzed between the frequency ranges of 20 kHz and 120 kHz, shows a reasonable agreement with the expected values. This provides us a great deal of confidence in utilizing this model to analyze the set up. There are dominant frequency components at the expected values as well as their third harmonic frequency values. There are some additional components as well (such as around 105 kHz) which need further analysis.

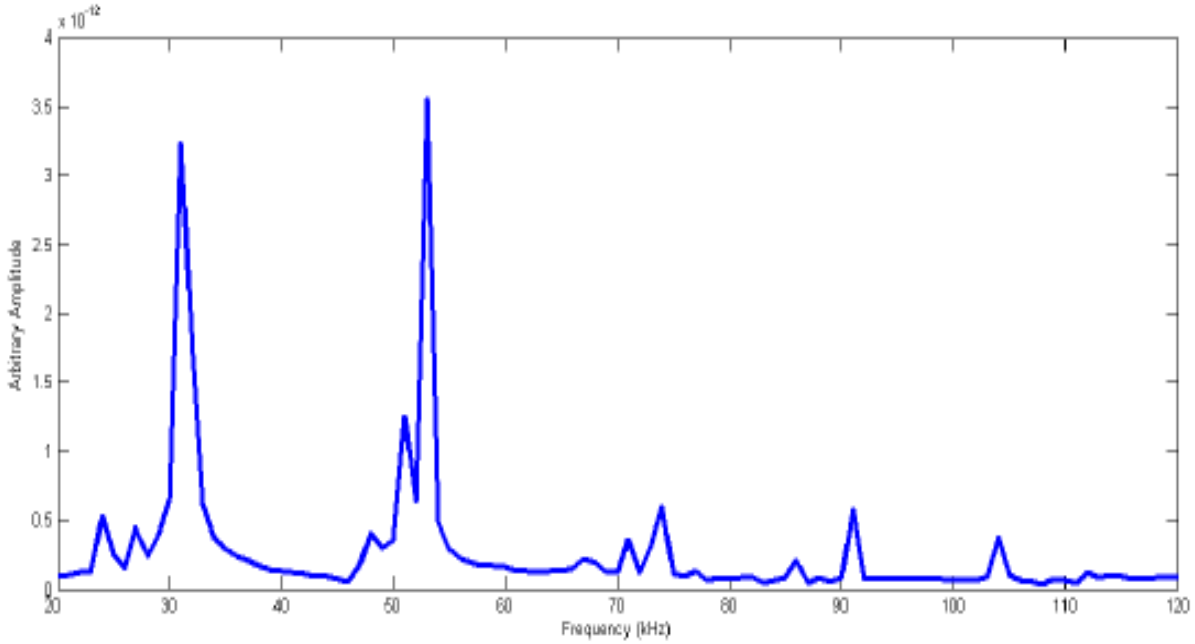

Fig. 13: Transient analysis of the set up

(b) Matching Layer Thickness

The frequency range chosen (20 kHz – 120 kHz) includes the first harmonic frequency of the PZT transducer as well as the Aluminum cylinder (32 kHz) and also their third harmonic frequency (96 kHz). The “quiet” cork matching layer was chosen to couple ultrasound from the container wall into the air medium inside the container. The convention when selecting matching layer thickness is chosen to be a quarter of the wavelength of sound wave. The quarter-wavelength thickness of the matching layer was calculated to be 0.79 mm. Therefore, off-the-shelf “quiet” cork of 0.8 mm thickness was purchased and was used in the experiments. Simulations were carried out to identify the changes in the frequency components based on the thickness of the matching layer. The following graph shows the effect of varying the matching layer thickness on the frequency components and also their contribution towards the peak displacement amplitudes in the target material inside the container. In Fig. 14 it can be seen that the maximum displacement was observed for 0.8mm thick matching layer at frequency of 93 kHz. Different matching layers seem to generate their respective maximum displacement amplitudes at different frequencies: 4 mm at 53 kHz; 2 mm at 108 kHz etc. This provides us with an idea of optimizing the matching layers in any given scenario. Knowing the container configuration, and based on the frequency requirements, the right thickness of the matching layer could be chosen from these results.

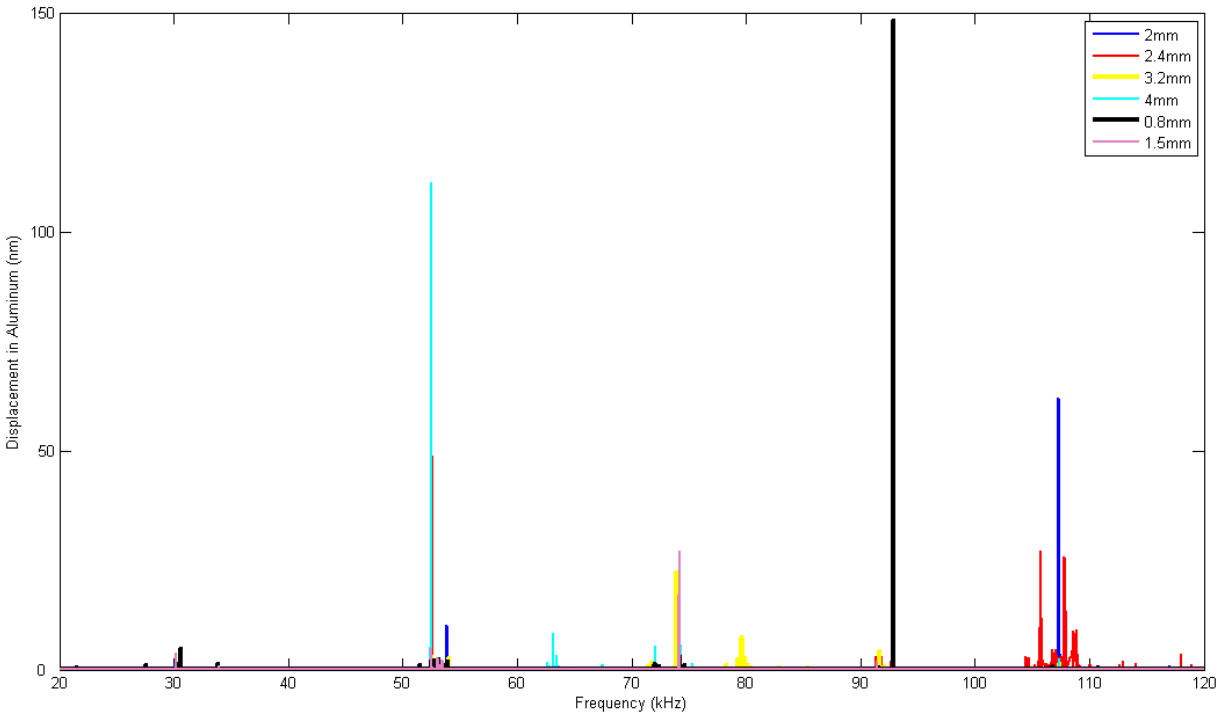

Fig. 14: Effect of matching layer thickness on experimentally observed acoustic displacements in the specimen

(c) Effect of Pressurizing the Container

It is well known that air is a highly attenuative medium during the transmission of ultrasound. However, this loss of energy could be overcome by pressurizing the propagating medium. Simulations were performed to understand the effect of the pressurized media on the displacements observed in the target material. It was assumed that the velocity of sound in air stayed approximately constant even after the pressurization. This was done to calculate the change in density of the medium. This was then incorporated into the finite element model.

The following plot shows the acoustic displacements in the Aluminum target specimen and the corresponding frequency components for two different pressure levels, atmospheric pressure (14.5 psi) and 750 psi. It can be seen in Fig. 15 that peak displacements are almost doubled with the increasing pressure but the dominant frequency components change due to the pressurization. The contribution to the lower frequency components is an interesting phenomenon and needs further work to be explained clearly.

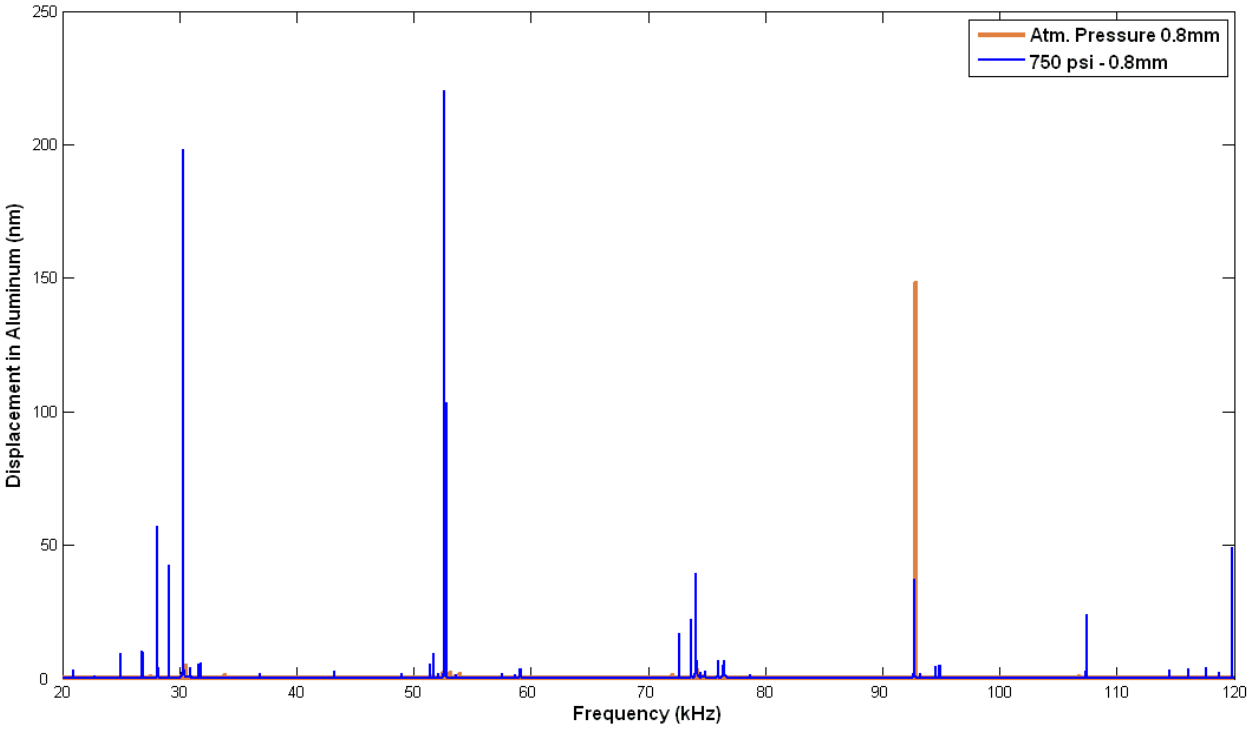

Fig. 15: Effect of the pressurized propagation medium (air) on transmitted acoustic displacements

Further simulations were performed to understand the effects of the variation of the container wall thickness as well as the introduction of an Aluminum plate to hold the transducer in place while attached to the container wall. It was generally seen that these variations caused changes to the frequency components of the observed displacements, as expected. The goal of the experiments is to ensure that the simulations mimic reality as closely as possible. Towards this end, the different parameters of the finite element model are altered to generate a set up that reflects the characteristics of the actual experimental set up. This is an ongoing process and once this is accomplished, and specific experimental verifications are obtained to validate the model, there will not any more need for conducting experiments which are extremely time-consuming.

(d) Correspondence between experiments and simulations

Since the experiments entail the use of sinusoidal waves to couple acoustic energy in to the container, all the analysis here on utilized a feature of the simulation, known as “Harmonic Analysis”. In this, the set up is analyzed for a broad range of frequencies (20 – 120 KHz, typically) where at each frequency step, sinusoidal acoustic waves are transmitted from the transducer and the response is studied by observing the displacements in the target material inside the container. The input signal amplitude was 100 V in these simulations.

The following plot compares the displacements observed (experimental as well as simulated) in the target material (Aluminum) inside the container at a pressure of 750 psi while a cork matching layer of 0.8mm thickness was used. There are quite remarkable coincidences in the frequency components. This provides us with a great deal of confidence in the 2-D axisymmetric model solved utilizing CAPA. However, further work

needs to be carried out in refining the model in terms of adjusting the damping parameters of the materials utilized in the model, incorporation of the three-point specimen holder etc. This however would involve three dimensional modeling; work is underway on that front.

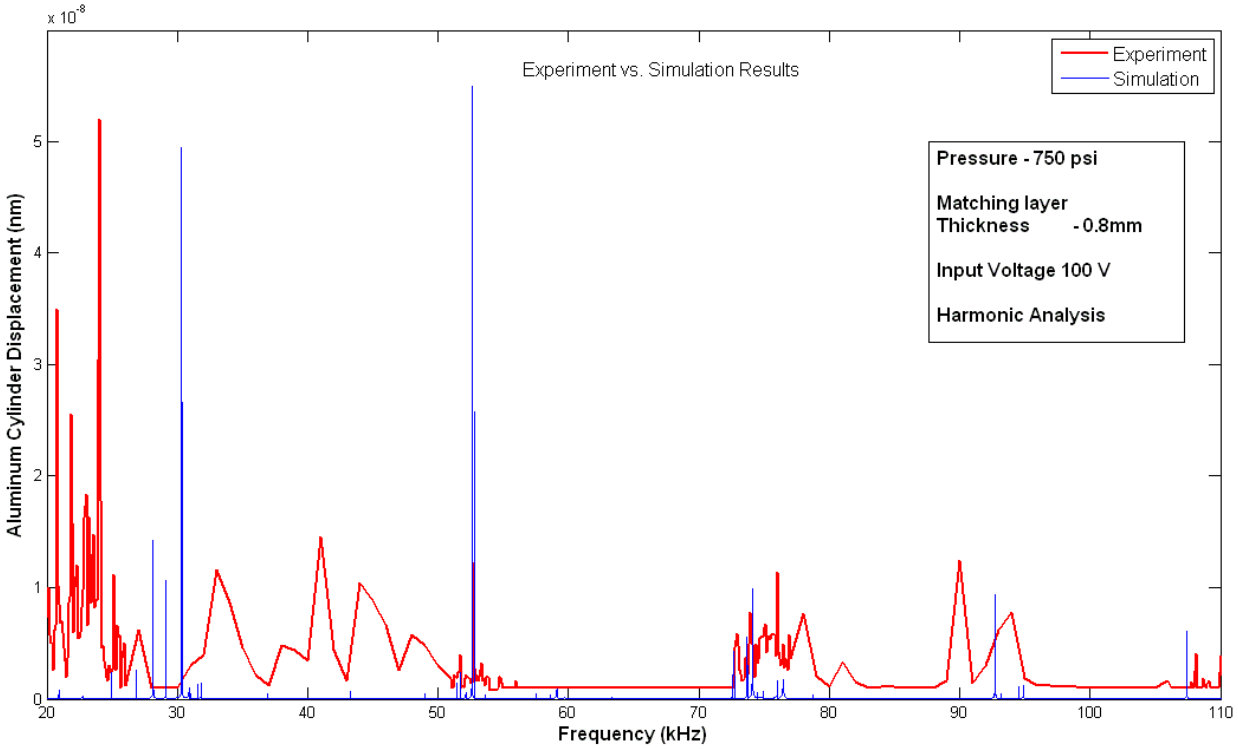

Fig. 16 Qualitative Agreement between Experimental and Simulation Results

SUMMARY

The primary objective of the project was to interrogate non-intrusively the target material and characterize it. To that end, the power of ultrasound was to be used to excite the nuclear and electron spins of the target material, to achieve the respective resonances. However, it is common knowledge that sound, especially in ultrasonic frequency regime, attenuates rather drastically when traveling through air. Therefore, the idea of pressurizing the chamber that contains the target material was put forth, as air when pressurized, tends to attenuate lesser than at atmospheric pressure.

Theoretical calculations were made to determine the nuclear and electron spin resonance frequencies of Aluminum, at earth's magnetic field (~0.54 G). They are 599.57 Hz and 1.511 MHz respectively. Ultrasonic PZT stack transducers were acquired to impart acoustic energy at the required frequencies to the Aluminum specimen. Power amplifiers were used to increase the amount of acoustic strain imparted to the specimen. A Laser Doppler Vibrometer (LDV) was utilized to obtain measurements of strain in the Al specimen.

It has been shown in literature that nuclear acoustic resonance could be observed by monitoring the nuclear spin-phonon absorption coefficient. When acoustic waves are transmitted into the specimen, there is absorption of energy by the nuclear spin system at the nuclear resonance frequency. LDV would be monitoring the vibration of the specimen during the frequency sweep. There is an inherent attenuation of transmitted acoustic energy due to the specimen vibration, however, when the NAR frequency is reached, there would be increased attenuation. By continuously monitoring the attenuation using the LDV, we would be able to observe NAR in Aluminum and other specimens.

Initial experiments were performed to determine the Quality factor (Q-factor) of ultrasound transmission using the PZT stacks into the Al specimen at frequencies of concern to us. Although the numbers were low, efforts were made to modify the experimental set up, such as the specimen holder, to increase the Q-factor. Radial displacement distributions in the specimen were also measured using the LDV to understand the extent of uniformity of displacements throughout the specimen. These results were then compared with simulations and the correlation was satisfactory.

Coupled Acoustic-Piezoelectric Analysis (CAPA) is a very powerful solver of Finite Element models constructed using ANSYS for acoustic energy transmission models. The different parameters that have been studied so far, using CAPA are:

5. The effect of matching layer thickness on the transmission of ultrasound into the pressure vessel, and its dependence on frequency.
6. The effect of the thickness of the end-cap of the pressure vessel: This was done to explore the idea of not using matching layers and instead use the correct thickness of the end-cap to maximize the transmission of acoustic energy into the target specimen.
7. The effect of the pressure inside the vessel on the displacements induced in the Al specimen.
8. The overall frequency characteristics of the entire experimental set-up.

Experiments have been conducted already to determine the efficacy of using a Finite Element model to simulate the air-coupled transmission of ultrasound at higher pressures. The initial results are very encouraging as there is sufficient matching between experiments and simulations. However, the model itself needs to be further refined in terms of incorporating experimental conditions such as three-point specimen holder etc.

Some of the immediate work will be involving the investigation of the effects of the Al specimen being wrapped in different materials such as plastic wraps, paper etc. Further confidence obtained from the matching of experimental and simulated results would aid us in performing simulations in a variety of target materials and also simulated many different situations, such as the vessel made of wood etc.

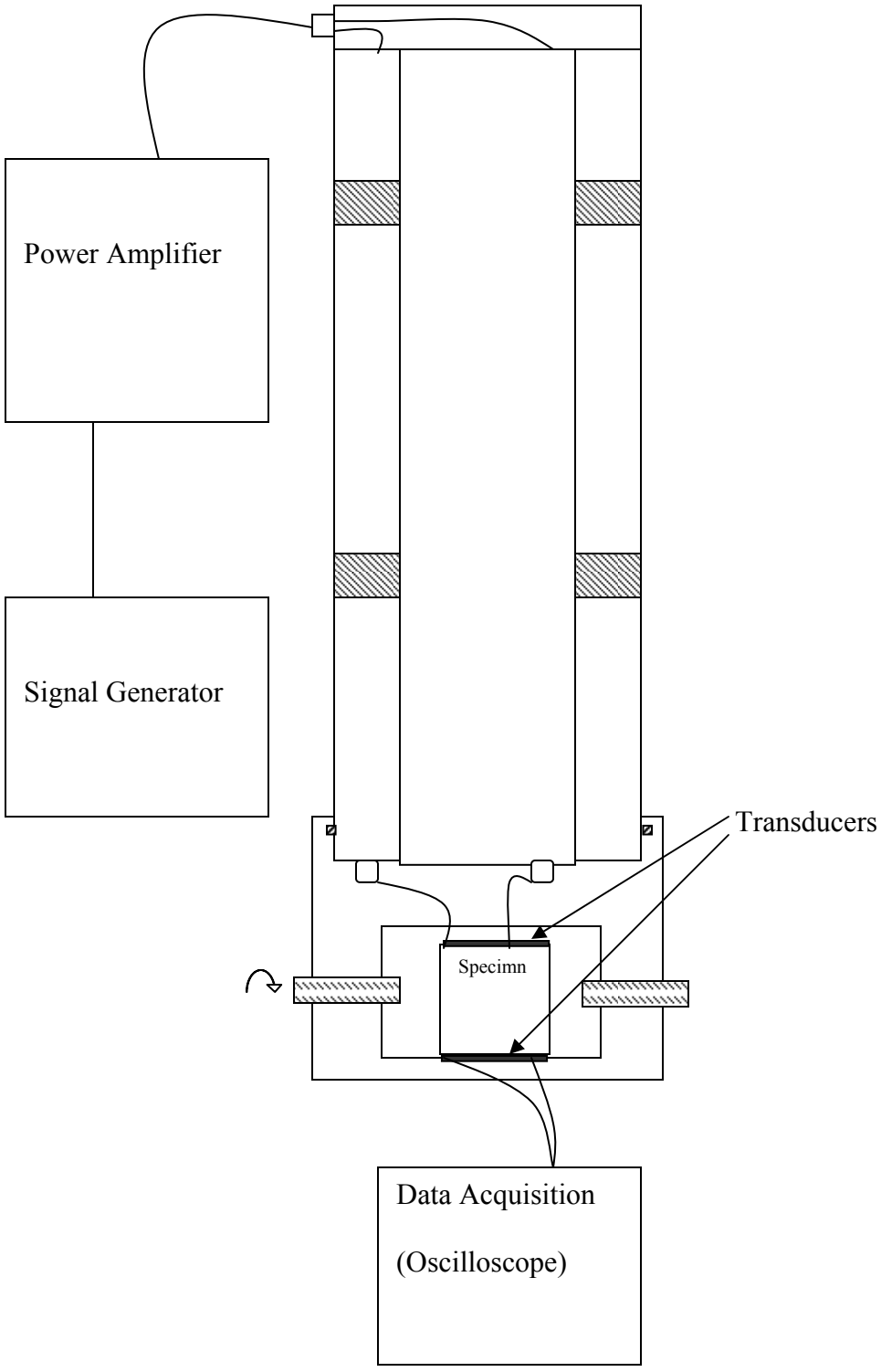
Power Amplifier
Signal Generator
Transducers
Specimn
Data Acquisition
(Oscilloscope)

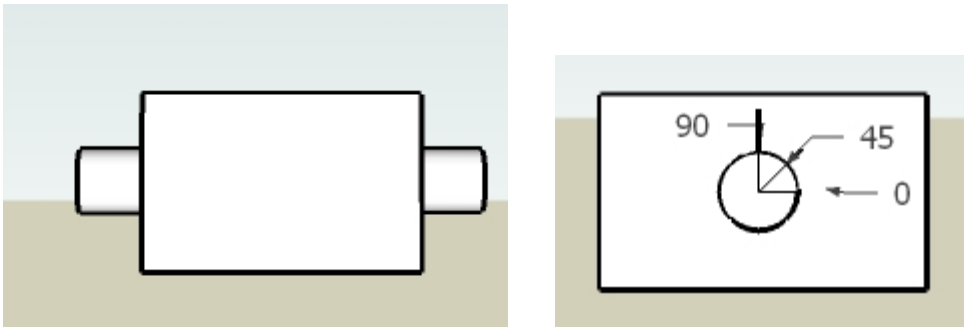

front view side view

Figure 17. Probe Design showing the leads, specimen holder, specimen, transducers and the associated electronics.

The specimen holder will have to be placed in the area of the modified NMR probe as shown in the probe design sketch. Essentially, it will be a Plexiglas box with top open (preferably) for specimen loading and the necessary connections to the transducers that could be attached to the specimen.

1. The dimensions of the Plexiglas box would be a direct resultant of the amount of space available inside the probe. From the dimensions provided in the schematic, it could be a maximum of 2" but since the design entails two cylindrical rods/spindles that are attached to the sides of the Plexiglas box, the box should be no more than 1" wide. It can be a cubical box.
2. The box + spindle will have to be placed in the area marked "specimen holder" using holes that are diametrically opposite, in the 4" high concentric pipe like fitting at the bottom.
3. We need to graduate the spindle circumference in terms of angles (0 degrees, 30, 45, 60 and 90) so that we can determine the acoustic absorption coefficient's dependence on the angle between the acoustic wave vector and the magnetic field.
4. From literature (Buttet, Gregory, Baily, 1969), while conducting NAR experiments with longitudinal waves, the least effect happens when the acoustic wave vector and the magnetic field are parallel. That is to say, in this NMR probe set-up, the magnetic field is vertically oriented and the transducers will be mounted on the top surface of the specimen. This is no good for us. Therefore, we need to attach the transducers on the left and right side faces of the specimen (refer to the front view of the Plexiglas box). Also, it should be noted that the maximum effect (in terms of acoustic absorption coefficient) occurs around 45 degrees.
5. The spindles will have to fit just snug into the holes so that we do not have to worry about holding the box in the required orientation. The friction between the spindle surface and the holes should take care of that. If that could not be the case, we could have threaded spindles and we shall use nuts on either side to secure the set up.

Specimen Requirements:

1. Since the amount of space available severely restricts the size of the specimen, we cannot utilize the single crystal Aluminum sample we already possess. We'll need a new sample.

2. Shape of the sample:
    a. While using transmitter and receiver transducers to monitor the acoustic absorption: In this case, the specimen could very well be cylindrical (however, the advantage of using a cubic sample could be understood from (b)). Since we need to attach the transducers to the parallel faces and observe the attenuation of acoustic energy sent in to the sample from the transmitter as we approach resonance, it becomes imperative that the specimen needs to be well polished and the faces need to be extremely parallel. (Certain literature suggest the end faces are flat within 1 micron and also to be within ±1° of the (100) crystal plane.
    b. While using Laser Doppler Vibrometer (LDV) to observe NAR: The LDV is capable of detecting out of plane displacements only. Therefore, using a cylindrical sample complicates the incidence of the laser beam from the LDV. This is where the use of Plexiglas comes in handy. The LDV could be positioned under the magnet and there is a clear optical path to the specimen. Another thing of importance is that, with this set-up, shear (transverse) waves will be used to excite the nuclear spin resonance in the specimen. The transducer can be attached to the left (or right) side of the sample and the out-of-plane displacement would be normal to the incident laser beam. The acoustic absorption coefficient is expected to be maximum when the acoustic wave vector and the magnetic field are parallel, i.e. 0°. (Buttet et al, 1969).

3. Bonding of transducer to the specimen: Non-aqueous stopcock grease from Fisher Scientific Company has generally been used in these experiments for temperatures below 230 K. For temperatures above it, Dow Corning High Vacuum grease has been used for bonding purposes.

4. The transducers that will be utilized in these experiments usually come in the following diameters: ¼", 3/8" and ½". It is preferable to use ½" diameter transducers as the ease of handling is better with increasing size. Since we'll be using ½" diameter transducers, the specimen preferably could be a cube with an edge size of 3/8". The transducer wafers will be chrome-and-gold plated to which the leads could be attached.

Items for Experiments

1. Specimen (to be provided by LLNL)
    a. Possible options – Aluminum, Vanadium, Copper, Lithium, Tantalum
    b. Single crystal
    c. Ends polished to optical flatness
    d. shape (cubical preferred)
    e. size (0.5" – 1")

2. Transducers (provided by PSU)

    a. A pair of transducers to work at 7.1 T. We'll take advantage of the higher harmonics to excite NAR in target specimen
    b. Electroded
    c. Modes of excitation – Longitudinal, Shear and combined modes
    d. Leads attached
    e. Transducer made of Lithium Niobate from Boston Piezoelectric
    f. Diameter (0.5" – 1")

3. Bonding Glue (PSU)
    a. For low temperature: NonAq grease from Fisher Scientific

4. Signal Generators (Available at PSU but Do we have to get clearance for the equipment that we may have to bring from PSU to the labs in LLNL?)
    a. Wavetek that has frequency and amplitude control and applicable up to 100 MHz
    b. Frequency sweep automation available using LabView - developed in our lab at PSU

5. Amplifiers (PSU)
    a. We have 2 broadband high power amplifiers with ability to work from 110 Hz to 100 MHz easily. However, they are heavy and cumbersome. Is it possible to use Power Amplifiers available at LLNL itself? Otherwise, we'll have to ship these out.

6. Data Acquisition (PSU)
    a. Tektronix digital multi-channel oscilloscope available with us. As with other equipment, what could we use that's available there itself to avoid shipping things out
    b. Automated frequency sweep software has the ability to save the reflected and transmitted signals from transducers
    c. Signal processing using auto-correlation and to identify absorption of energy at resonance

Attenuation Coefficient Calculations

When sound waves were applied to the metal, it induced the motion of charged particles, which in the presence of an applied magnetic field (B_o) are deflected and set up transverse currents, which in turn, generate electromagnetic field propagating at the speed of sound. The amplitude of the component of B in a plane perpendicular to B_o is given by,

$B_\perp = \varepsilon B_o f(\theta)$

where $f(\theta)$ is an angular factor depending on the polarization of the sound wave. In case of longitudinal wave, it is $sin\theta\ cos\theta$ and for shear wave propagating along the z-direction and polarized in the x-direction, it is $cos\theta$ and when the shear wave is polarized in y-direction, $f(\theta)$ is $cos^2\theta$. Utilizing the equation for acoustic power per unit volume, they deduced the acoustic absorption coefficient to be,

$$\alpha_n = \frac{\pi^2 h^2 NF(I)g(\nu)\nu^4}{4kT\rho\upsilon^3}\left[f(\theta)\right]^2$$

where *F(I)* is a spin factor given by

$$F(I) = \frac{1}{2I+1}\left[2I^2(I+1) - \sum_{m=-I+1}^{I} m(m-1)\right]$$

For the case of Single Crystal Aluminum specimen (I = 5/2), at room temperature (300 K), and using 20 MHz shear (transverse) waves propagating in the [0 0 1] direction:

Size of the cubical Aluminum specimen, 1 cm^3 (assumed).
Therefore, the total number of atoms (N) = 87 x 10^{21} since the volume of one Al atom could be calculated using its radius (1.4 Å).

The spin factor F(I) for this case (I = 5/2) is 7.25.
Shear velocity in Aluminum = 3270 m/s
Density of Aluminum = 2700 Kg/m^3

$f(\theta) = 1$

The line-shape is assumed to be Gaussian. $\int_0^\infty g(\nu)d\nu = 1$

The acoustic attenuation coefficient (α_n) is calculated to be approximately 1.7 x 10^{-5} /cm.

The NAR frequency is assumed to be 20 MHz. Therefore, the assumed magnetic field would be in the range of 2T. However, the NMR instrument generated a constant field of 7.1 T and the corresponding NAR frequency in Aluminum would be 77.7 MHz. The attenuation coefficient would also change accordingly. The above calculation was performed to provide a check with an already existing calculation in literature.

References:
[1] J.E. Zimmerman, J.A. Cowen, and A.H. Silver, *Applied Physics Letters*, **10**, 5, 142-145 (1967)
[2] website: http://www.dhushara.com/book/explod/nuclears/nuc.htm
[3] D. L. Bolef and R.K. Sundfors, *Nuclear Acoustic Resonance, Academic Press*, Harcourt Brace & Company, NY, 1993.
[4] R. Kubo and Tomita, K.J., *J. Phy. Soc. Jap*., **9**, 888-919 (1954)
[5] D.I. Bolef and M.Menes, *Physical Review*, **114**, 6, 1441-1451 (1959)
[6] A.H. Silver and J.E. Zimmerman, *Applied Physics Letters*, **10**, 5, 142-145 (1967)
[7] P.A. Fedders, *Physical Review B*, **1974**, 1740-1743, (1973)
[8] R.A. Webb, *Rev. Sci. Instrum.,* **48**, 12, 1585-1594 (1977)
[9] K.S. Pickens, G. Mozurkwich, D.I. Bolef, and R.K. Sunfords, *Physical Review Letters*, **53**, 2,156-159(1984)

[10] K.S. Pickens, D.I. Bolef, M.R. Holland, and R.K. Sunfords, *Physical Review B*, **30**, 3644-3648 (1984)

Appendix I
Table of Relevant Properties of some Isotopes

Note: Resonance frequencies are quoted relative to a resonance frequency of exactly 100 MHz for 1H.

Tantalum

Isotope: 181Ta

Spin:	7/2
Natural abunance:	99.988 %
Magnetogyric ratio (rad/T s):	3.22 x 10^7
Relative receptivity:	3.65 x 10^-2
Magnetic moment	2.66
Quadrupole moment Q/m(2)	3
Resonance frequency	12.0 MHz

Aluminum

Isotope: 27Al

```
Spin:                          5/2
Natural abundance:              100 %
Magnetogyric ratio (rad/T s): 6.9760 x 10^7
Relative receptivity:          0.207
Magnetic moment                4.3084
Quadrupole moment Q/m(2)       0.15
Resonance frequency            26.077 MHz
```

Isotope: 7Li

```
Spin:                          3/2
Natural abundance:              92.58 %
Magnetogyric ratio (rad/T s): 10.3975 x 10^7
Relative receptivity:          0.272
Magnetic Moment                4.20394
Quadrupole moment Q/m(2)       -4 x 10^-2
Resonance frequency            38.836 MHz
```

Copper

Isotope: 63Cu

```
Spin:                          3/2
Natural abundance:              69.09 %
Magnetogyric ratio (rad/T s): 7.0974 x 10^7
Relative receptivity:          6.45 x 10^-2
Magnetic moment                2.8696
Quadrupole moment Q/m(2)       -0.211
Resonance frequency            26.530 MHz
```

Isotope: 65Cu

```
Spin:                          3/2
Natural abundance:              30.91 %
Magnetogyric ratio (rad/T s): 7.6031 x 10^7
Relative receptivity:          3.55 x 10^-2
Magnetic moment                3.0741
Quadrupole moment Q/m(2)       -.0195
Resonance frequency            28.421 MHz
```

Uranium

Isotope: 235U

```
Spin:                          7/2
Natural abundance:              0.72 %
Magnetogyric ratio (rad/T s):
Relative receptivity:
Magnetic moment
Quadrupole moment Q/m(2)
Resonance frequency            1.790 MHz
```

Vanadium

Isotope: 51V

```
Spin:                          7/2
Natural abundance:              99.76 %
Magnetogyric ratio (rad/T s): 7.0453 x 10^7
Relative receptivity:          0.383
Magnetic moment                5.8379
Quadrupole moment Q/m(2)       -5 x 10^-2
Resonance frequency            26.336 MHz
```

Appendix II
Spin Relaxation Time Calculations

A) From Dr. Overhauser's doctorate thesis "Studies in the electron theory of metals", the **electron spin relaxation time due to interaction with the nuclei** of the metal is given by:

$$\tau = \frac{27\hbar^3 I}{256\pi m \kappa_o N \mu^2 \mu_N^2 (I+1)\left|\psi(0)\right|^4}$$

where μ is the Bohr Magneton (= 9.274015 x 10^{-21} JT^{-1}), μ_N is the nuclear magneton (= 5.050787 x 10^{-27} JT^{-1}), m – the mass of an electron (9.109390 x 10^{-31} kg), and for lithium metal (I = 3/2), $|\psi(0)|^2$ =34.

From Overhauser's thesis (page number 13), the Fermi energy for electrons in lithium is 4.7 eV and this corresponds to wave number K_o of 1.11 x 10^8 per cm.

Number of spins per cc (N) calculation:

Atomic Volume: 13.1 cc /mol, that is 6.023 x 10^{23} atoms (or spins since each lithium atom has one free electron). Therefore, N = 6.023 x 10^{23} / 13.1 = 4.597 x 10^{22} per cc.

On page 28, Dr. Overhauser has calculated this relaxation time to be **1.9 x 10^{-4} s**. However, later on in the thesis (page 79), he has introduced a correction factor of 60, and the final corrected

relaxation time is τ =1.14 x 10^{-2} s.

B) **<u>Relaxation due to interaction with spin currents</u>** (magnetic dipole moments)

From Page 47, the relaxation time is given as:

$$\tau = \frac{9m^2c^4\hbar}{20e^4K_o^2\kappa T \log(\frac{\kappa T \in^{1.5}}{\mu H})}$$

where $\in$ = 2.718 eV (difference in Fermi energies of spin up and spin down states, for lithium). Therefore, for a magnetic field of 5 Gauss and a temperature of 293 K,

In the Dr. Overhauser thesis the relaxation time has been calculated as 7.9 x 10^{-7} s in the thesis and the corrected value is

τ =1.3 x 10^{-3} s.

Milestone Status Table:
Milestone Status Table:

ID Number	Task / Milestone Description	Planned Completion	Actual Completion	Comments
1	Validate Proof of Principles and Develop Demonstration System			
1.1	Numerical Estimates of Acoustic Strain Needed to Drive Aluminum Nuclear and Electron Resonance	10/30/04	10/30/04	Completed
1.2	Optimization of Overhauser Effect Magnetometer System Sensitivity	02/15/05	2/15/05	Completed
1.3	Development of Magnetic Shielding Techniques	05/15/05	5/15/05	Completed
1.4	Optimization of Acoustic Energy Coupling	11/30/06	11/15/08	Completed
1.5	Development of Strain Measurements	09/15/06	11/15/08	Completed
1.6	Demonstration that Electron Spin Resonance Can be Achieved	12/30/08	11/15/08	Completed
1.7	Demonstrate Discrimination Between Materials	02/28/09	11/15/08	Completed
1.8	Numerical Determination of Acoustic Strain Needed to Drive Uranium Resonance	04/30/09	11/15/08	Completed
2	Development of Miniaturized Prototype System	12/15/08	11/15/08	On schedule
2.1	Perform NAR with Potassium Magnetometer	05/15/007	11/15/08	Completed
2.2	Implement Digital Lock-in Amplifier Computer	11/15/06	11/15/08	Completed
2.3	Integrate Ultrasound Radiation with Detectors Using LabView	09/15/06	11/15/08	Completed
2.4	Interpolate NAR Results (Uranium and Plutonium Samples)	11/15/08	11/15/08	Cancelled
2.5	Double Resonance Experiments in Non-Contact Mode	09/15/06	09/15/06	Completed
3	Alternate Techniques for NAR			
3.1	Development of SQUID detectors as a detector	04/15/05	04/15/05	Completed
3.2	Development of SQUID detectors to investigate how much ultrasonic energy is needed to drive the nuclei and electrons in a particular sample	09/30/05		Task cancelled due to equipment problems.

Budget Data (July 31, 2008):

Phase / Budget Period			Approved Spending Plan			Actual Spent to Date		
			DOE Amount	Cost Share	Total	DOE Amount	Cost Share	Total
	From	To						
Year 1	5/17/04	5/16/05	185,000	55,000	240,000	185,000	55,000	240,000
Year 2	5/17/05	5/16/06	180,000		180,000	180,000		180,000
Year 3	5/17/06	7/31/08	100,000		100,000	100,000		100,000
Year 4								
Year 5								
		Totals	465,000	55,000	520,000	465,000	55,000	520,000

Spending Plan for the Next Year: Not Applicable